SAND79-8196
UC-62d
Unlimited Release

INVESTIGATION OF FREE-FORCED CONVECTION FLOWS IN CAVITY-TYPE RECEIVERS

Joseph A. C. Humphrey
Frederick S. Sherman
Patrick Le Quere
Kang-Shin Chen
Lori Miller
Wai-Ming To
Department of Mechanical Enginerring
University of California
Berkeley, California

Printed January 1982

DISCLAIMER

SAND--79-8196

DE82 010034

SAND79-8196
Unlimited Distribution

INVESTIGATION OF FREE-FORCED CONVECTION FLOWS IN CAVITY-TYPE RECEIVERS

FINAL YEARLY REPORT (1979-1980)
TO SANDIA LABORATORIES, LIVERMORE
CORRESPONDING TO RESEARCH CONTRACT No. 20-1012

by

Joseph A.C. Humphrey, Principal Investigator
Frederick S. Sherman, Co-Principal Investigator
Patrick Le Quere, Visiting Research Associate
Kang-Shin Chen, Research Graduate Student
Lori Miller, Research Graduate Student
Wai-Ming To, Research Graduate Student

Department of Mechanical Engineering
University of California
Berkeley, California 94720

October 1980

ABSTRACT

A summary is provided of the first of three years of experimental and theoretical research on free-forced convection flows in cavity-type solar receivers. New experimental and theoretical results are presented and discussed. The implication of these findings, with respect to the future thrust of the research program, are clarified as well as is possible at the present time. Following various related conclusions a summary and tentative schedule of work projected for year two of research is presented.

CONTENTS

		PAGE
1.	SUMMARY OF RESEARCH ACCOMPLISHMENTS FOR YEAR ONE (1979-1980)	1
	1.1 Experimental work	3
	1.2 Theoretical work	5
2.	NEW EXPERIMENTAL RESULTS AND DISCUSSION	8
3.	NEW THEORETICAL RESULTS AND DISCUSSION	11
4.	CONCLUSIONS	13
5.	SUMMARY AND PROJECTED RESEARCH SCHEDULE FOR YEAR TWO (1980-1981)	15
	5.1 Experimental work	15
	5.2 Theoretical work	16
ACKNOWLEDGEMENTS		18
REFERENCE		19
TABLES		23, 24
FIGURES		21, 22, 25, 26
APPENDIX: "Numerical Calculation of Thermally Driven Two-Dimensional Unsteady Laminar Flow in Cavities of Rectangular Cross-Section", by P. Le Quere, J.A.C. Humphrey and F.S. Sherman, Mechanical Engineering Report No. FM 80/1, University of California, Berkeley		27

1. SUMMARY OF RESEARCH ACCOMPLISHMENTS FOR YEAR ONE (1979-1980)

In this section an overview is provided of the first of three years of experimental and theoretical investigation of free-forced convection losses from a laboratory-scale model of a solar thermal cavity-type receiver.

The main purpose of this work is to develop, over a three-year period, a numerical calculation procedure capable of predicting two-dimensional, recirculating, unsteady, free-forced convection turbulent flows. Heat transfer conditions are such that the Boussinesq approximation does not apply. A characteristic demanded of the calculation scheme is that at a later date it should be easily extended to allow the prediction of more general three-dimensional flows.

A stage-wise approach has been taken in the study by delineating specific objectives to be met during the three-year program. Year one, briefly reviewed below, has been devoted to developing and testing a laminar version of the calculation scheme. Years two and three will be devoted to extending the applicability of the numerical procedure to turbulent flow and (particularly during year three) exploring its adaption to large scale cavity geometries.

It is mandatory that in the course of its development the calculation scheme should be tested rigorously. For laminar flow this has already been done by reference to data available on flat plate and enclosure geometries. Similar information does not exist for cavity-type geometries for the heat transfer and flow conditions of interest to this work. This has led to the incorporation of a substantial experimental effort in the study which is being conducted in parallel with the theoretical-numerical work. The experiment consists of a laboratory-scale electrically heated cavity geometry

of variable orientation and aspect ratio. Temperature levels from ambient to about 1000°F can be uniformly maintained at two heated inside cavity walls. Although several orders of magnitude removed from life-size devices in terms of attainable Grashof and Reynolds numbers, the small-scale experiment provides quantitative temperature and velocity information, as well as qualitative features of the flow obtained by means of the shadowgraph technique. The data is indispensable for testing the calculation scheme thoroughly. It is particularly important to learn how to impose far-field flow conditions in the free-convection flow regime. This can be found from experimentation.

The remainder of this section is divided into two parts, corresponding to the experimental and theoretical accomplishments of year one respectively. A rather substantial account of much of the work performed during year one of research has already been provided in the form of a mid-term report (July 1980) to Sandia Laboratories. The report includes an extensive literature review, covering experimental and theoretical studies of flat-plate, enclosure and open-cavity flows with thermal effects of relevance to this work. In an effort to avoid unnecessary duplication, throughout the remainder of this communication reference will be made to the mid-term report as the need arises.

1.1 Experimental work

An experimental apparatus has been constructed and tested, a) to help clarify the complex fluid mechanic and thermal processes taking place in high temperature open cavity flows and b) to serve as a test base for validating the calculation procedure for this class of flows. The apparatus and its associated instrumentation have been described in the July 1980 mid-term report. A brief summary is given below.

Existing literature provided little help for the design of the experimental equipment. This accounts, in part, for the delays incurred during its fabrication. In the final design, the cavity has a fixed length-to-height ratio (frontal view) equal to 5.70, to encourage two-dimensional mean flow. The cavity cross-section (side view) is rectangular, with a continuously variable depth-to-height aspect ratio ranging from 0 (flat plate conditions) to 1.40 (deepest cavity condition). The cavity is 23 3/4" long and 3 11/16" high.

Side walls made of 1/8" borosilicate glass plates allow optical probing of the cavity along its length (span-wise direction). Strip heaters imbedded in the bottom and back inner cavity walls allow temperatures of about 1000°F to be achieved at these walls. To date the apparatus has been tested at a maximum wall temperature of 750°F. Cruciform arrays of thermocouples on each of the three inner walls permit monitoring of temperature conditions there.

The heated inner walls of the cavity are made of 1 1/4" thick copper plate. The non-heated wall is 1/4" thick copper. These walls are surrounded by not less than 2" thick Fiberfrax Duraboard insulation. The main frame supporting the copper plates and insulation is made of 1/4" aluminum plate - except for end walls which are 1" thick. A steel harness, allowing for

variable cavity orientation, pivots on brackets mounted on the aluminum end walls. The whole of the test section is supported by a steel stand. This stand has a pulley arrangement which allows tilting of the cavity between -60 and +60 degrees with respect to gravity.

Experiments corresponding to free-convection regime in the cavity are presently being performed. These are described in section 2 of this report. Free-forced convection experiments have been moved from year one to year two of research and will be carried out in the Mechanical Engineering Department subsonic wind tunnel. Carpentry and electric power modifications to the wind tunnel have been completed which allow the inclusion of the cavity and its stand in the large chamber preceeding the contraction section. Glass windows on the sides of the wind tunnel allow optical access at the level the cavity will stand. The windows are large enough so that cavity cross-section and orientation may be varied over full ranges while the cavity remains within the field of view.

Testing of the apparatus has been concluded. It has been verified that all aspects of mechanical design and electrical operation (heaters, power control units and thermocouple measurements of temperature) are in working condition.

1.2 Theoretical work

The development and testing of the numerical procedure was accomplished by subdividing the work of year one into sequential tasks. The framework serving as the algorithm basis for this study was the two-dimensional, elliptic, steady state TEACH calculation procedure from Imperial College, London. Prior to extending the procedure to encompass the class of flows of interest here the TEACH code was streamlined and debugged. The conservation equations modeled in the original algorithm were then extended to include unsteady terms. This required that the solution algorithm be modified in order to be able to calculate iteratively in the time domain.

The complete set of conservation equations modeled in the new algorithm, their origin and justification and their applicability to this work have been discussed in detail in the July 1980 mid-term report. Suffice it to remark here that the equations describe those types of flows wherein high frequency pressure oscillations are neglected but large thermal variations are allowed. Thus, while the equations are not Boussinesq-approximated, density is essentially a function of temperature only. This avoids the time-step limitations imposed in any numerical effort to trace sound waves. Rigorous forms are used for the momentum and continuity equations. Auxiliary relations for physical properties and the ideal gas law close the system of equations modeled.

Testing of the expanded code, henceforth referred to as REBUFFS*, was rigorously conducted with particular emphasis placed on thermally driven laminar flow along flat plates and in rectangular enclosures. The results and discussion of the validation process are carefully detailed in the July 1980 mid-term report.

---

*Acronym for: Recirculating Buoyant and Forced Flow Solver.

The validated scheme was applied to predict thermally driven flow in open cavities of rectangular cross-section. To do this it was necessary to prescribe appropriate far-field conditions for velocity and temperature. In the first set of calculations, normal derivatives of temperature and velocity at the far-field boundaries were set equal to zero; except for temperature which was set equal to the ambient value at the bottom inlet far-field plane. Numerical experimentation showed that the cavity flow was insensitive to perturbations purposefully induced on the far-field boundaries. This is due to the strong local determination of flow in the cavity. Nevertheless, in an effort to produce a more realistic picture of the far-field flow a different far-field boundary specification for velocity was used. The approach (together with results and discussion,) is described in the appendix and is based on the notion that the far-field flow should be both incompressible and irrotational.

Among the desireable new features included in the REBUFFS code is an improved differencing technique for convection terms in the transport equations. The use of quadratic upstream interpolation as opposed to hybrid differencing permits stability of the calculation scheme for high values of the Peclet number while retaining second order accuracy in the computations. The procedure and its improvements are documented in the July 1980 mid-term report. It should be remarked that the higher order scheme appears to resolve time-dependent recirculating structures in open cavity flows in more detail, at a given value of Grashof number, than the hybrid scheme.

A matrix of open cavity flow calculations has been provided in the July 1980 mid-term report for the following ranges of relevant parameters: $10^4 \leq Gr \leq 3 \cdot 10^7$, ΔT = 50 and 500K, a/b = 1/2, 1 and 2, and Pr = 0.73. Flow field calculations are in good qualitative agreement with the cavity-flow

visualization results obtained so far, although the latter appear more unsteady than the former. It will be especially important to establish experimentally the nature of the far-field flow in order to determine the most appropriate treatment of velocity components at the far-field boundaries.

In summary, a time-dependent, two-dimensional, elliptic flow calculation procedure has been developed. It has been found that an appropriate formulation of the far-field boundary conditions is required in order to predict the far-field of an open cavity flow. However, local events inside the cavity are essentially independent of far-field conditions if the latter are imposed at a distance far-enough removed from the cavity (typically about two cavity widths). The calculations verify the strong dependence of velocity and temperature on geometry cross-section and inclination. Quantitative checks between predictions and measurements of the temperature field are necessary and underway.

2. NEW EXPERIMENTAL RESULTS AND DISCUSSION

The experimental component of this work is now under way in full force. Some of the results obtained to date, for free-convection are presented here. A work schedule for the experimental program during year two, including the free-forced convection flow regime, is tabulated in section 5 of this report.

Typical flow visualization results obtained using the shadowgraph technique are shown in Figure 1. These correspond to a cavity aspect ratio of one, with the cavity tilted to 0, 20 and 45 degrees, respectively. The shadowgraphs were obtained by shining an intense point source of light from a xenon tube along the spanwise length of the cavity. The magnified image projected onto a piece of vellum (drafting) paper, was photographed with a movie camera and with a 35mm SLR camera. The movie films* immediately convey a "feeling" for the scale and intensity of the fluid motion which is not apparent in the still photographs shown in the figures.

Time-averaged measurements of wall temperature were taken at the positions defined in Figure 2 and Table 1. The data for a nominal temperature of 400°C, and air aspect ratio a/b = 1, is shown in Table 2 for three angles of the cavity, α = 0°, 20° and 45°. As expected, the temperature of each wall is very nearly uniform. This is true even of the top wall, which contains no heaters and receives heat only from the air in the cavity and, by conduction and radiation, from the heated back and bottom walls. Thus, in the numerical calculations, we may accurately impose boundary conditions of uniform temperature on each wall.

A most interesting characteristic of the cavity flow is the inherent instability of the boundary layer generated on the bottom wall by the flow entering the cavity at the aperture plane. The shadowgraph technique sharply delineates the region of interaction between the heated boundary layer fluid and the cold fluid entering the cavity. It is remarkable that, in spite of

*These are available at a cost covering duplication and postage to destination.

very careful attempts to ensure a purely free-convection regime*, for all the experimental conditions the boundary layer "flaps"; the flow separating from the sharp lower lip of the cavity is unstable and will oscillate, even at very low Grashof numbers. At high Grashof numbers, the numerical calculations show oscillations in this same general region, but it seems that the frequencies of experimental and computed oscillations are quite different.

The position of zero velocity in the aperture plane is a weak function of cavity orientation as is shown by the plot given in Figure 3 .

For all orientations the flow entering the cavity is considerably more streamlined than that emerging. Buoyancy driven motions along inclined walls, especially the back wall, cause mixing of the flow. For downward facing orientations a large eddy, the size of which increases with inclination angle, is trapped at the upper wall corner. Thermal stratification in the inclined orientations appears to stabilize the flow. Nevertheless, lumps of heated fluid are seen to emerge sporadically from the cavity. Whether this is a predictable time-evolving process governed by the equations of two-dimensional motion, or a random, turbulence related, phenomenom, is not clear at the time of writing.

Numerical calculations reveal the existence of two large recirculation zones or eddies in the cavity for α = 45 degrees. The flow visualization results appear to confirm this prediction although for conditions which do not correspond exactly to the calculations.

Measurements of temperature in the aperture plane have not yet been obtained. In principle a resistance thermometer made of fine tungsten wire could yield measurements of temperature which would not require corrections

---

*The cavity is protected from sideways ventilation by a tent-like enclosure made of cloth which allows entrainment of air through the bottom and its exit through the top.

due to radiation and convection-induced thermal losses. However the construction of such a probe appears to be difficult and costly and its viability is presently being assessed. In the meantime, a chromel-alumel thermocouple probe spanning the length of the cavity is being checked as a possible alternative for making measurements of temperature in the aperture plane. Two probes of different wire diameter are being tested. Some preliminary data for the larger diameter probe (0.030") are shown in Figure 4. The temperature plot shows qualitatively correct trends. An estimate of the amount of error incurred in the measurements is indicated in the figure. Thus, in the aperture plane at the location where flow enters the cavity the thermocouple should have measured ambient temperature but radiation and convection errors combined have produced a reading 7.5°C in excess of this value. Theoretical calculations based on an error analysis given in appendix A8 of the mid-term report predict a reading error of 35% for a wire 0.030" in diameter. The error estimated from Figure 4 is about 31%. The error analysis indicates that a wire 0.003" in diameter would be subject to an uncertainty of about 20%. Measurements of temperature will be made with this wire thickness to demonstrate the viability of the thermocouple approach as a suitable alternative to the original resistance thermometer proposal.

3. NEW THEORETICAL RESULTS AND DISCUSSION

In the July 1980 mid-term report a considerable amount of numerical information was provided concerning the flow and temperature fields within a heated open cavity. The results were presented as vector velocity and temperature plots for a range of Grashof numbers (10^4, 10^5, 10^6 and 10^7), two dimensionless temperature differences, ($\Delta T/T_\infty$ = 50/288 and 500/288), and an aspect ratio of one. The fluid properties were those for air and were taken as functions of temperature with T_∞ = 288°K (except for the specific heat at constant pressure).

A preliminary discussion of these results was also provided in the report. However, since the submission of the report, new computations have been performed. They are included here with a detailed discussion and are presented in the form of an appendix. A summary of important findings is listed below.

1. Accurate far field specifications of boundary conditions for velocity are necessary for resolving properly the flow field in front of the cavity opening. However, the flow field <u>within</u> the cavity is essentially insensitive (for the conditions computed) to the far field boundary condition specifications provided these are sufficiently removed from the aperture plane (about two cavity heights).
2. The quadratic upstream interpolation technique appears to be superior to the hybrid difference technique for convective terms. The former reveals time dependence of the flow, which is suppressed by the numerical diffusion of the latter.
3. Cavity aspect ratio and inclination angle strongly influence heat losses for fixed Grashof number and temperature difference. In

general the mean Nusselt number increases with Grashoff number, and is larger for shallow cavities than for deep. This is especially the case when the cavity is tilted down. A tabulation of the various parameters affecting heat transfer is given in the appendix.

Presently, calculations are being performed for experimental conditions of cavity flow with free convection. The question of what is the most appropriate treatment of far field boundary conditions is also being considered. Both these issues will be addressed in a future communication.

Finally, it has been found in the numerical work that for high Grashof numbers ($Gr \gtrsim 10^7$) the calculation procedure requires under-relaxation of buoyancy effects to ensure stability. This, however, means that it takes longer for the procedure to satisfy a pre-established convergence criterion and, consequently, that the calculations are more costly.

4. CONCLUSIONS

The following major conclusions may be drawn from the work accomplished during the first year of this research project.

1. There is, to date, no body of fundamental experimental data pertaining to thermally driven flow in open cavities of simple geometry (with or without forced convection effects superimposed) which serves the purposes of: a) helping to understand the fluid mechanical and thermal processes taking place; b) guiding the modeling of those flows, especially in turbulence regime; c) testing the worthiness of possible calculation schemes.
2. A laboratory scale experimental apparatus has been constructed and tested which will alleviate the situation pointed out in 1. above. Preliminary flows visualization results and temperature measurements are in qualitative agreement with predictions in free-convection regime.
3. A quantitative technique for measurement of temperature using 0.003" chromel-alummel thermocouple probe is being tested for substitution of the originally proposed resistance thermometer concept.
4. A two-dimensional, transient, non-Boussinesq calculation procedure, the REBUFFS code, has been developed, tested and applied to vertical plate, open and enclosed cavity flows in laminar regime. A solution procedure capable of predicting general thermally driven cavity flows is very desirable since, if it can be used with confidence, it is considerably more economical to run than the equivalent amount of experimentation. The REBUFFS code can readily be extended to encompass three-dimensional flows. During year two of research it will be generalized to predict two-dimensional turbulent flows.

5. Both experiment and calculations show that the flow field in an open cavity can be time-dependent and that the recirculating nature of the flow is a strong function of cavity aspect ratio, orientation and $\frac{\Delta T}{T_\infty}$ at fixed Gr. The influence of variations in these parameters can be systematically investigated with a calculation scheme over the ranges of Grashof and ΔT for which it is reasonable to expect laminar flow.
6. Currently further development of the scheme is underway to allow stably convergent calculations at high values of the Grashof number.

5. SUMMARY AND PROJECTED RESEARCH SCHEDULE FOR YEAR TWO (1980-1981)

The numerical component of this research has progressed satisfactorily and is presently on schedule. The calculation of experimental test cases has been postponed until experimental data is available but a matrix of relevant test cases has been computed and documented, in part, in the July 1980 mid-term report pertaining to this contract. Current efforts are being dedicated to reviewing literature related to the turbulence modeling approach to be pursued in this work (see original proposal for details concerning the model).

By contrast to the numerical work the experimental component of the study has been set back relative to the schedule originally anticipated. The main cause for the delay has been the construction of the apparatus which has proven to be an elaborate and sophisticated piece of equipment.

Flow visualization and temperature measurements have been commenced in free-convection regime. Flow visualization and temperature measurements in free and free-forced convection modes will be conducted prior to point-wise measurements of velocity in free-convection regime.

5.1 Experimental Work

The main tasks to be accomplished under this heading during year two of research are:

1) Completion of flow visualization and temperature measurements of cavity flow in free convection regime.
2) Commencement and completion of flow visualization and temperature measurements of cavity flow in free-forced convection regime.
3) Commencement and completion of point-wise measurements of velocity of cavity flow in free and free-forced convection regimes. Additional measurements of temperature to correlate with velocity results.

It is anticipated that use will be made of an existing dual velocity component laser-Doppler velocimeter facility linked to an automatic data acquisition system run by a PDP 11/34 minicomputer. It is fairly clear how the facility can be used to make the free convection measurements of velocity. However, the use of the facility for obtaining corresponding measurements in the free-forced convection regime requires further consideration since the wind-tunnel, wherein the cavity will be placed for the forced convection experiments, is at a considerable distance from the velocimeter's location. It is very unlikely that the rather large velocimeter facility can be disassembled and transported to the wind-tunnel site. It currently serves five on-going experiments* where it is presently located and for which it was originally conceived. Alternate ways of measuring velocity in and about the cavity when in the wind tunnel are being considered; among them laser-Doppler velocimetry with a similar but more portable system, vane anemometry and streak photography.

5.2 Theoretical Work

In parallel with the experimental work further development of the calculation code for predicting open cavity two-dimensional flows will be pursued. Aspects of the code which require further development and testing are:

a) Inclusion of forced convection in the flow

b) Inclusion of turbulence in the flow and its modeling

c) Formulation of appropriate density weighted transport equations

While point (a) is fairly simple to deal with, point (b) will require careful investigation and a relative evaluation of turbulence closure models of relevance to cavity flows with free-forced convection effects. Guidance

*Including the free convection cavity flow regime of interest to this work.

exists in the literature concerning possible paths for developing (b) and (c) above. A detailed exposition of the turbulence modeling approach most likely to be pursued in this work has been given in the original proposal.

It is quite likely that the development and testing of (a), (b) and (c) above will run into year three of research. Development and testing of the turbulence model will be guided not only by present experimentation but by existing data relating to cavity flows and cavity experiments such as the one being conducted by Dr. J. Kraabel and associates at Sandia Laboratories, Livermore. Finally, it should be noticed that further developments of the calculation procedure, its testing and extended runs will be performed on the CDC 7600 machine at the Lawrence Berkeley Laboratory.

5.3 Comment on Changes in Manpower

A new Ph.D. graduate research student, Mr. Wai Min To, has been selected to continue with the numerical and turbulence modeling aspects of the work. Mr. Kang Shin Chen will continue with the experimental component of the study with the assistance of Ms. Lori Miller (M. Sc. Candidate).

Professor Sherman will be on sabbatical leave during the Winter and Spring quarters 1980-81 but will be available for consultation in relation to this research.

ACKNOWLEDGEMENTS

This research would not have been possible without the continued and varied support received from several individuals who are strongly linked to the investigation.

Our thanks go to the Mechanical Engineering Department machine shop and electronics staff who performed an outstanding job in building and instrumenting the laboratory-scale cavity receiver model. We are especially indebted to Robert Cesarello and Peter Dale who have been very closely connected with the experiment. Encouragement and helpful suggestions provided by Dee Davis, Lou Grout and Al Shaw are gratefully appreciated.

Frequent discussions with M. Abrams, R. Gallagher, J. Kraabel and S. Paolucci of Sandia Laboratories have led to critical and very constructive appraisals of this study throughout the various stages of its execution. We continue to look forward to future, mutually beneficial, discussions.

Special thanks are due to Taeyoung Han who throughout the first year of this program of research provided considerable insight bearing on the formulation of the numerical problem. We are grateful to him for his very valuable contribution.

REFERENCE

Humphrey, J.A.C., F. S. Sherman, P. Le Quere and K. Chen. "Investigation of Free-Forced Convection Flows in Cavity-Type Receivers." Mid-term report for Sandia Laboratories, Livermore Contract No. 482447 26984-4. July 1980.

THIS PAGE LEFT INTENTIONALLY BLANK.

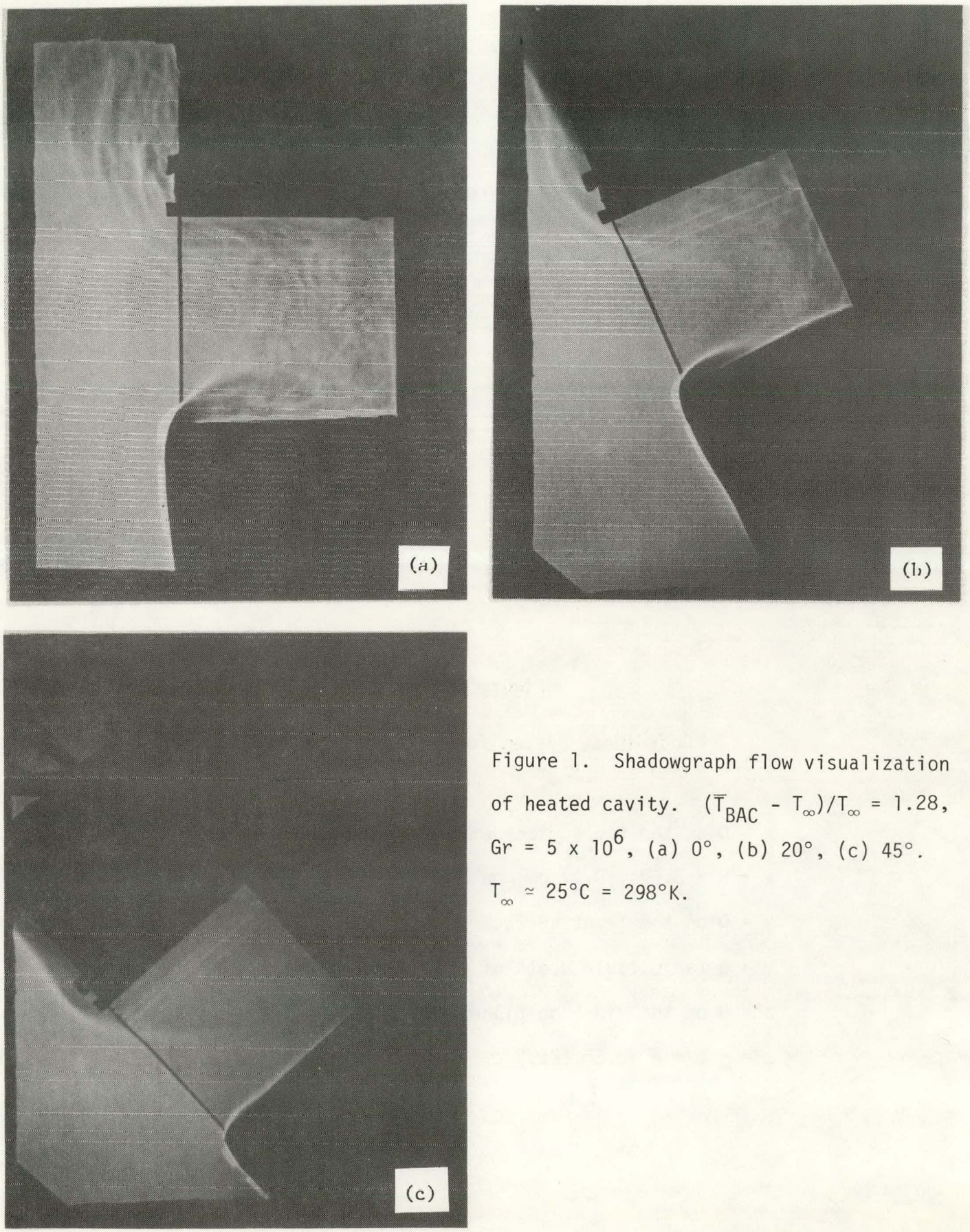

Figure 1. Shadowgraph flow visualization of heated cavity. $(\overline{T}_{BAC} - T_\infty)/T_\infty = 1.28$, $Gr = 5 \times 10^6$, (a) 0°, (b) 20°, (c) 45°. $T_\infty \simeq 25°C = 298°K$.

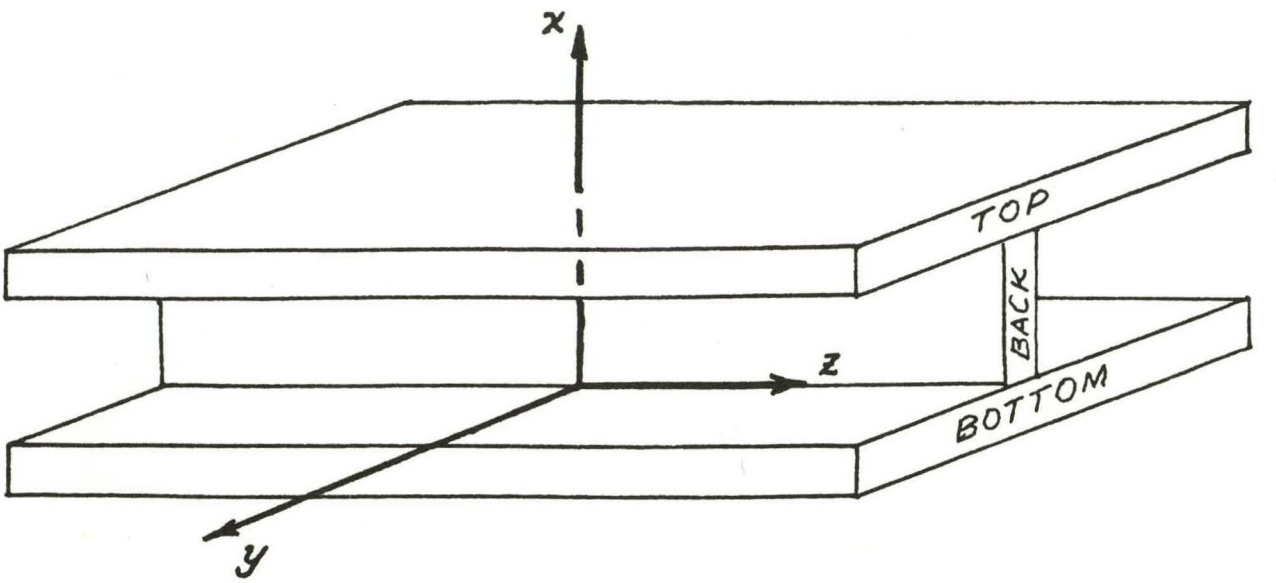

Figure 2

Coordinate System for Model Cavity

x = 0 on the top surface of the bottom wall.

x = b = 3.69" (9.37 cm) on bottom surface of top wall.

y = 0 on the front surface of the back wall.

y = a (adjustable depth of cavity) on aperture plane.

z = 0 on the mid-span plane.

z = $\pm$ c = $\pm$ 10.5" (26.7 cm) on the side planes.

T.C.#	x (inches)	a-y (inches)	z (inches)	NOTES
0	0	0.22	0	Bottom Wall
1	0	2.88	0	
2	0	6.25	0	
3	0	9.20	0	
4	0	4.56	-2.50	
5	0	4.56	2.50	
6	0	4.56	-5.00	
7	0	4.56	5.00	
8	0	4.56	-7.50	
9	0	4.56	7.50	
10	1.25	a	0	Back Wall
11	3.50	a	0	
12	2.38	a	-2.50	
13	.38	a	2.50	
14	2.38	a	-5.00	
15	2.38	a	5.00	
16	2.38	a	-7.50	
17	2.38	a	7.50	
18	3.69	0.28	0	Top Wall
19	3.69	1.75	0	
20	3.69	3.25	0	
21	3.69	4.81	0	
22	3.69	6.38	0	
23	3.69	7.86	0	
24	3.69	9.35	0	
25	3.69	4.81	-2.50	
26	3.69	4.81	2.50	
27	3.69	4.81	-5.00	
28	3.69	4.81	5.00	

Table 1

Locations of Wall Thermocouples
(See Figure 2 for Definition of Coordinates)

T.C. #	α = 0°	α = 20°	α = 45°	Notes	
0	395°C	385°C	390°C	exposed to flow	
1	399	390	397		
2	403	397	412		
3	403	397	417		
4	400	393	408		
5	400	393	404	behind	Bottom
6	396	391	400	back	
7	398	391	402	wall	
8	394	387	397		
9	394	388	399		
10	393	398	400		
11	392	398	400		
12	398	395	398		
13	393	399	401		
14	dead	dead	dead		Back
15	392	398	401		
16	382	386	389		
17	390	396	399		
18	333	337	342		
19	328	335	340	exposed to flow	
20	333	339	344		
21	338	344	348		
22	335	340	345		
23	325	332	338	behind	
24	330	334	339	back	
25	336	342	346	wall	Top
26	341	346	351		
27	331	337	341		
28	345	351	356		

Table 2

Typical Surface Temperatures

a = b = 3.69

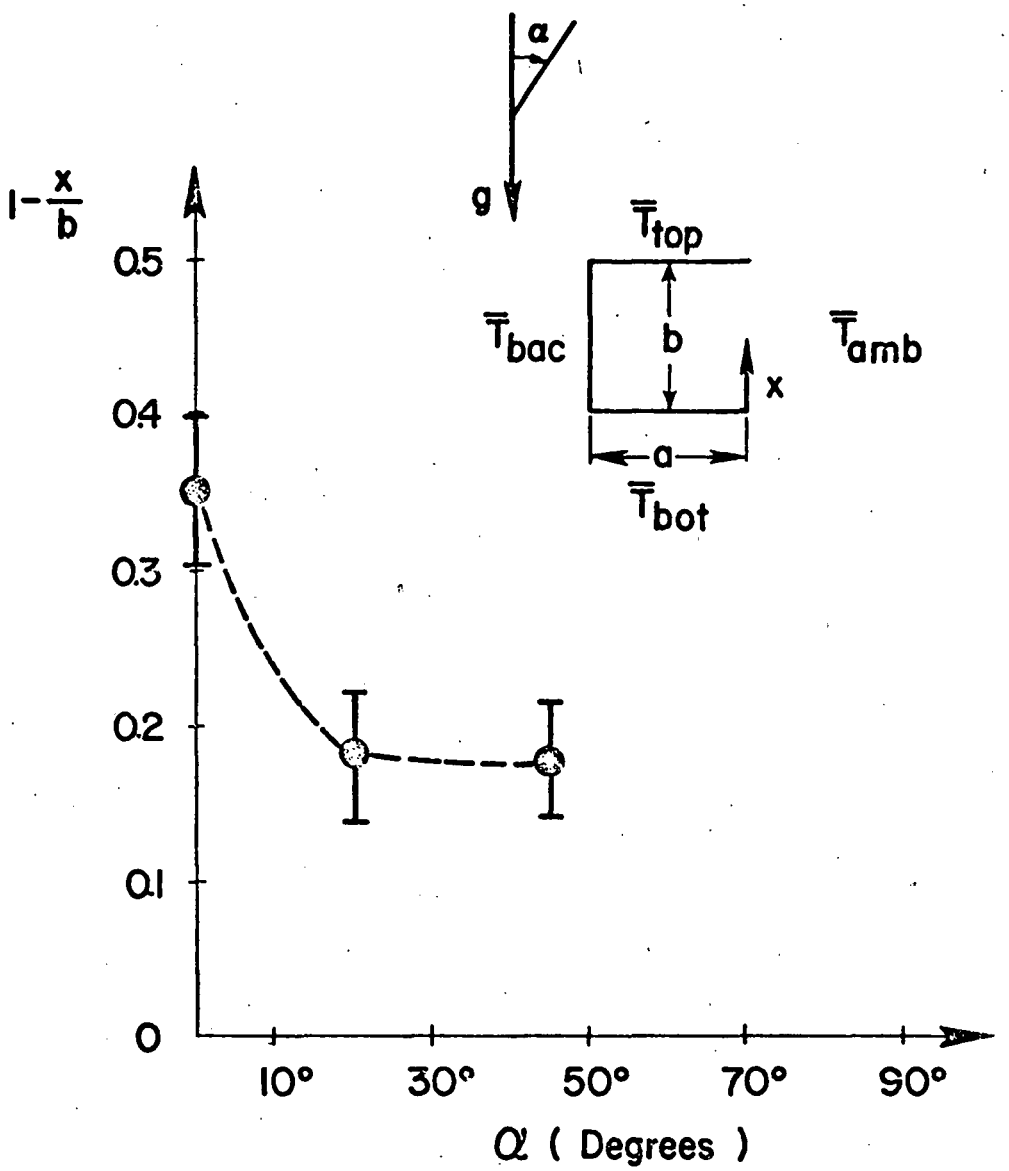

Figure 3. Approximate location of zero velocity position on aperture plane: a/b = 1 (b = 9.37 cm); $\overline{T}_{bot}$ = 402 ± 10°C; $\overline{T}_{bac}$ = 400 ± 4°C; $\overline{T}_{top}$ = 348 ± 4°C; $\overline{T}_{amb}$ = 23°C = 296°K; $Gr = g\beta(\overline{T}_{bac} - \overline{T}_{amb})b^3/\nu^2 = 5 \times 10^6$; β and ν evaluated at $T_f = (\overline{T}_{bac} + \overline{T}_{amb})/2$.

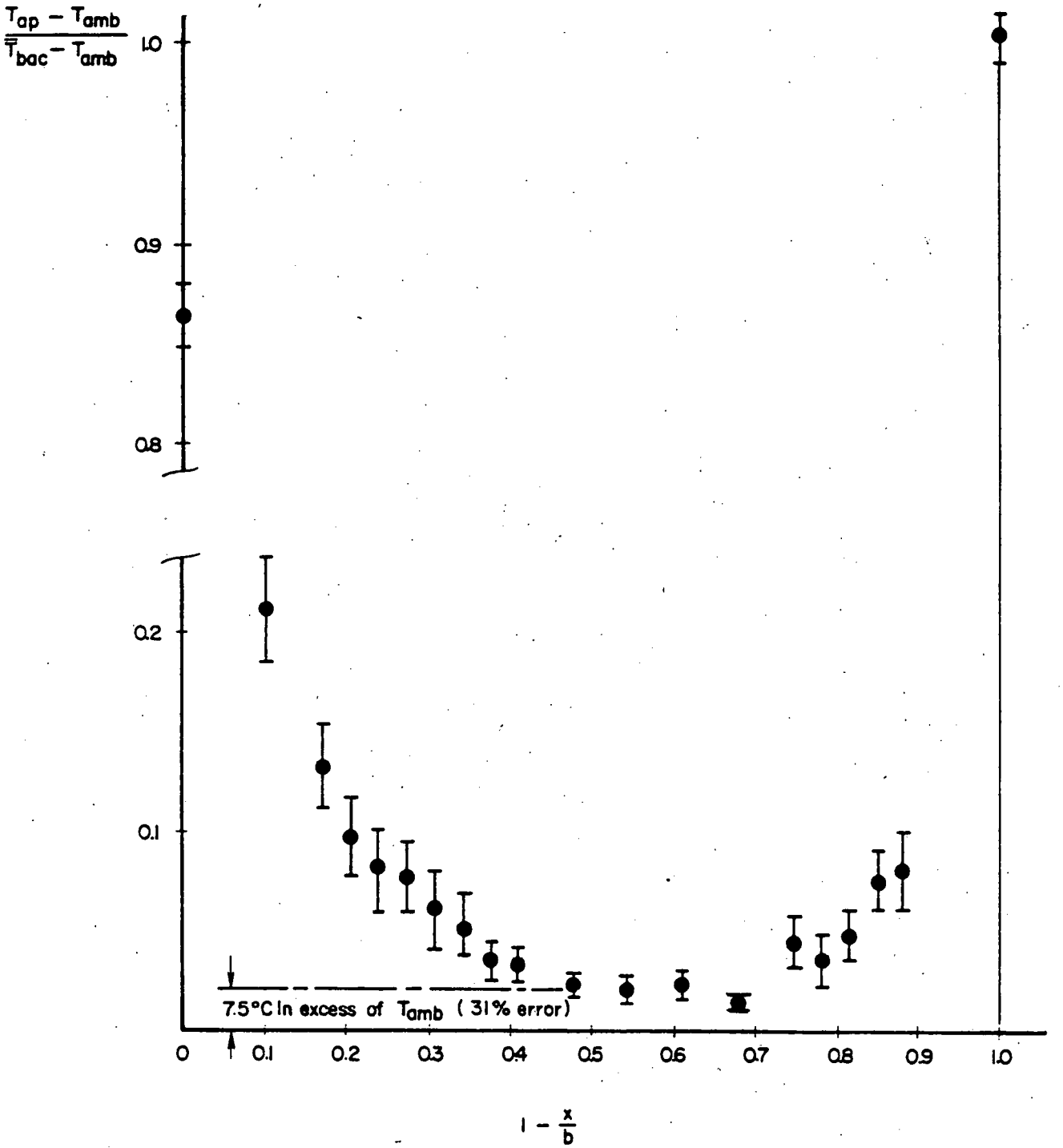

Figure 4. Temperature profile in aperture plane using 0.030" Chromel-Alumel thermocouple wire; a/b = 1, α = 0; average wall temperatures, Grashof number and geometry specified in Figure 3.

APPENDIX

"Numerical Calculation of Thermally Driven Two-Dimensional Unsteady Laminar Flow in Cavities of Rectangular Cross-Section"

NUMERICAL CALCULATION OF THERMALLY DRIVEN TWO-DIMENSIONAL UNSTEADY LAMINAR FLOW IN CAVITIES OF RECTANGULAR CROSS-SECTION

by

Patrick Le Quere[1], Joseph A.C. Humphrey and Frederick Sherman

Department of Mechanical Engineering

University of California, Berkeley

Berkeley, California 94720

Report No. FM 80/1

Submitted to Numerical Heat Transfer

(May 1981)

---

[1] Present Address: Laboratoire d'Energetique Solaire
40 avenue du recteur Pineau, 86000 Poitiers, France.

ABSTRACT

Numerical results are reported for thermally-driven laminar flow in two-dimensional rectangular geometries with one plane, the aperture plane, removed. Finite difference expressions are derived from a set of approximated transport equations in which large temperature and density variations are allowed but high frequency pressure oscillations are not. The approach allows small time-step limitations to be removed from the calculation procedure. A second order accurate quadratic upstream interpolation technique is used for the finite differencing of convection terms in the transport equations thus reducing numerical diffusion error.

Parameters varied in the calculations were cavity aspect ratio and inclination angle with respect to gravity, inside wall temperature and Grashof number. A value of Prandtl number corresponding to air was fixed (Pr = 0.73).

The calculations reveal various and complex recirculating flow structures in the cavity which are a strong function of cavity aspect ratio and inclination angle. Thus, inclined cavities with a downward-facing aperture plane show one or two (counter-rotating) vortices, depending on the inclincation angle. Flow unsteadiness similar to that observed experimentally by Humphrey, et al. [31] appears at $Gr > 10^6$ and also depends strongly on the cavity geometrical characteristics and orientation. For cavities with the aperture plane aligned with the gravity vector, the unsteadiness appears as a periodic series of small "bubble-like" vortices which sweep the bottom cavity wall. These vortices are sequentially driven by the bulk convective motion of air entering the cavity towards the back wall where they rise. For downward-facing cavity flows the unsteadiness is dampened and appears not to exist for angles larger than 20 degrees and $Gr \lesssim 10^6$. In general, the results show that the average Nusselt

number of a cavity decreases with increasing aspect ratio and inclination angle and with decreasing wall temperature and Grashof number.

It is an interesting feature of the problem examined that, although the flow field approaching the cavity is a function of the type of far-field conditions specified, the flow fields within the cavity and in the aperture plane are determined mainly by local heat transfer events. Predictions of the cavity fluid mechani cand heat transfer characteristics are relatively insensitive to the far-field boundary condition specification provided it is made at a distance 1.5 cavity heights or more from the aperture plane.

Page

INTRODUCTION 1

The Problem of Interest 1

Non-Boussinesq Calculation Procedures 2

Objectives of This Study 5

GOVERNING EQUATIONS AND BOUNDARY CONDITIONS 7

THE NUMERICAL PROCEDURE 14

Finite Difference Equations 14

Calculation Scheme: the REBUFFS Code 19

Miscellaneous Matters 20

Validation 25

OPEN CAVITY RESULTS AND DISCUSSION 28

General Considerations 28

Velocity and Temperature Profiles 34

Heat Transfer Calculations 36

CONCLUSIONS 39

ACKNOWLEDGEMENTS 41

REFERENCES 42

TABLES

FIGURE CAPTIONS

FIGURES

NOTATION

A_j convection-diffusion coefficient in difference equation

a cavity depth dimension

b cavity aperture plane dimension

c_j mass flux through cell wall

c_p specific heat at constant pressure

G_j mass flux

Gr Grashof number $\left(\frac{g\beta(T_w-T_\infty)b^3}{\nu^2}\right)$

g_i acceleration due to gravity

k thermal conductivity

L length of vertical flat plate

M total mass in an enclosed cavity

m mass cell in balance

Nu Nusselt number (defined by equation 31)

Pr Prandtl number $\left(\frac{\mu c_p}{k}\right)$

p pressure

Ra Rayleigh number (Gr × Pr)

R^* gas constant for air

S source term in difference equation

T temperature

t time

u_i velocity component

v volume

α cavity inclination angle with respect to gravity vector

β coefficient of volume expansion

Γ transport coefficient in difference equation

Notation continued

ε dimensionless temperature perturbation parameter

μ viscosity

ν kinematic viscosity

ρ density

τ_{ij} stress tensor

ϕ dummy variable in difference equation

ψ stream function

Subscripts denote

C cold

d dynamic component

H hot

i ith component coordinate

j jth component coordinate

max maximum value

o initial value

P node P in the calculation domain

W wall value

x x component coordinate

y y component coordinate

∞ ambient value

Superscripts denote

$\bar{}$ average value

n time step n

* value of past iteration (within n)

** value of present iteration (within n)

' correction value

Symbols

Δ	finite increment
∇^2	Laplacian operator
Σ	summation

INTRODUCTION

The Problem of Interest

Flows driven by thermally induced buoyant forces, or which are significantly affected by buoyant forces, arise in many situations, both natural and man-made. Much effort has been expended in the experimental and theoretical study of these flows. The most extensively investigated geometry is almost certainly the semi-infinite flat plate, vertically aligned or inclined. Recently, considerable attention has been given to understanding better the problem of thermally driven flow in rectangular enclosures. These studies have been strongly motivated by the need to quantify the relative contribution of free convection to the heat transfer between a pair of facing vertical walls. Such a configuration is of relevance to, for example: cooling of nuclear fuel rods, ventilation and energy conservation in buildings, fire spread in rooms and corridors, reactor insulation, etc. A tabulated review of over 100 references pertaining to these flows is available in the report by Humphrey et al. [1].

Buoyant flows within and about cavities* with internal surfaces at high temperatures have received comparatively little attention, even though such heated cavities provide an attractive design option for Solar Thermal Central Receiver Systems (STCRS). These systems have been identified as a possible technological pathway for generating high-quality energy, essentially free of undesirable chemical pollutants, from a virtually inexhaustible source. However, it has been shown [2] that the performance and efficiency of a life-scale STCRS will be significantly affected by the thermal losses it sustains. Of these, the most difficult to quantify are

---

* Defined here as a rectangular enclosure with one face removed.

free-forced convection losses, which are comparable in magnitude to losses incurred through radiation effects.

Numerical calculations of thermally induced flows past cavities have been performed by Penot [3] and Orlandi, Onofri and Subetta [4], who used Boussinesq approximated equations and solved for streamfunction and vorticity. The results of these studies show clearly the importance of buoyant forces in cavity flow heat transfer. In particular, Penot [3] has demonstrated the dependence of thermal losses on cavity orientation as well as the existence of time-dependent large scale variations in the flow for specific conditions of Grashof number and inclination angle.

Non-Boussinesq Calculation Procedures

Because it reduces the number of dimensionless parameters on which the flow depends, the Boussinesq approximation is desirable. It cannot, however, be justified for the high energy flux flows of interest to this work, in which very large spatial variations in density occur. Only a few predictive studies of thermally driven flows in closed and open cavities have not employed the Boussinesq approximation. Several of these are briefly discussed below.

A perturbation approach, in terms of the parameter $\varepsilon = 2(T_H - T_C)/(T_H + T_C)$, was used by Rubel and Landis [5] for predicting thermally driven flows in enclosures. By developing the Navier-Stokes equations in a power series expansion in ε and retaining zeroth and first order terms, density variations were accounted for in the inertia terms. Thus, for example, these authors observed an asymmetrical shift of the

uni-cellular motion displayed by the streamfunction towards the lower colder corner of their enclosure.

Unfortunately, the power series expansion approach is severely limited by the need to provide and evaluate an increasing number of terms as ε increases. Consequently, methods based on a direct numerical approach are more appealing. It appears that Polezhaev [6] was the first to pursue a numerical approach based on an algorithm for high speed compressible flow. In Polezhaev's formulation time derivatives are retained in the Navier-Stokes equations and pressure is replaced by the product ρT wherever it appears. The calculation procedure involves using a two time-level step scheme fractional in space. Each of the four variables (u_x, u_y, T, ρ) is calculated separately from the rest, leading to independent tri-diagonal matrices. The solution of the equation system in this formulation requires eight intermediate steps in order to advance one full step in time. Polehaev's predictions are in good qualitative agreement with the results of Rubel and Landis [5] and Spradley and Churchill [7] for values of $Ra \lesssim 10^5$. Central differencing of convective terms and the artificial decoupling introduced by the sequential treatment of variables are the cause for poor results for $Ra \gtrsim 10^6$. Although mentioned in the paper, the restrictions imposed by high frequency acoustic phenomena and corresponding time step limitations are not discussed in detail.

Spradley and Churchill [7] have studied more completely the role of high frequency motions in thermally driven enclosure flows. They showed that heat is transferred by pressure waves which originate from a step change in temperature at time t = 0 at the heated vertical wall in the enclosure. However, their numerical scheme, like that of Polezhaev, was severely constrained by time step limitations.

In a study of three-dimensional enclosures, Le Quere and Alziary [8] avoid the time step limitation by using an implicit numerical scheme in which non-linearities in time are dealt with according to the Briley-McDonald [9] linearization procedure. The resulting equations are solved by the Douglas-Gunn [10] ADI procedure. Although the scheme is very stable, analysis of the formal truncation error due to factorization in space shows that it is useless to choose arbitrarily large time steps. Thus, the optimum time step was determined to be 100 times the CFL compressible limit.

The three numerical approaches outlined above apply to flows in which density and pressure variations are strongly coupled. They require small time steps to describe the propagation of pressure waves at acoustic speeds. In a less restrictive scheme, Leonardi and Reizes [11] solve elliptic forms of the momentum equations formulated in terms of streamfunction and vorticity using the false transient method developed by Mallinson and De Vahl Davis [12]. Although pressure is explicitly absent in the equations, in order to determine density from the equation of state they chose to solve a Poisson equation for pressure. This equation, together with the elliptic equation relating streamfunction to vorticity, makes it necessary to solve two Poisson equations per "time step", thereby impairing the efficiency of the scheme.

It has been shown by Rehm and Baum [13] that in very non-adiabatic, non-dissipative buoyant perfect gas flows wherein the time scale associated with heat addition and resultant fluid motion is necessarily long compared with the transit time of an acoustic signal across the enclosure, acoustic oscillations due to elastic properties of the fluid may be ignored. These authors derive a set of simplified time-dependent transport equations characterized by a spatially uniform mean pressure appearing in both the equations of energy and

of state, with the spatially non-uniform component of pressure appearing only in the momentum equation. Thus, in problems for which their formulation is accurate, pressure remains almost constant in space while density and temperature vary significantly. The arguments formally set forth in the analysis by Rehm and Baum were intuitively applied by Forester and Emery [14] and Ku, Doria and Lloyd [15] in respective elliptic calculation schemes which were formulated in terms of primitive variables and in which time dependent terms were retained. The enclosure calculations provided by Forester and Emery are mostly for $Ra = 10^4$ and were obtained using central difference approximations for the convection terms. The authors were interested in a cryogenic application and recognized that the extension of their calculation procedure to higher Rayleigh number flows would require an improved finite difference scheme for convection. The numerical procedure employed by Ku, Doria and Lloyd is based on a hybrid differencing scheme (upwind/central) for convection terms. As will be shown below, such a scheme yields accurate results for $Ra \lesssim 10^6$ provided sufficient grid refinement is used in calculating the flow field. However, this approach becomes expensive in terms of computational time and storage for larger values of Rayleigh number; an especially serious limitation in any calculation scheme, if, subsequently, it is to be extended to three-dimensional flows.

Objectives of This Study

The present work provides the first of several necessary steps towards predicting general free-forced recirculating flows in and about strongly heated cavities (open or closed) of variable orientation and aspect ratio.

The calculation procedure developed in this study is firmly based on an extension of the formal analysis of Rehm and Baum [13]. It is elliptic

in nature, but retains time dependence by treating transient terms as extra source terms in the formulation. Thus, for ranges of the variables for which a steady state solution exists, the solution can be calculated by simply setting a very large time step in the calculation scheme. The solution is then attained, iteratively, within this single time step. The implementation of a higher order difference scheme for convection terms, based on the quadratic upstream interpolation approach suggested by Leonard [16], allows accurate computations to be performed in convection-dominated flows with coarser grids than are allowed by an upwind/central hybrid difference approach. In particular, for high values of Grashof number ($Gr \gtrsim 10^6$) it has been found that more detailed resolution of the unsteady flow field is predicted by the higher order scheme. Finally, the procedure developed here (unlike that of Penot) solves for primitive variables directly and can readily be extended to predict three-dimensional, buoyant, time-dependent flows.

GOVERNING EQUATIONS AND BOUNDARY CONDITIONS

The set of elliptic partial differential equations governing a single-phase, compressible, variable property flow is given below in (repeated) sub-indexed notation form.

Continuity

$$\frac{\partial \rho}{\partial t} + \frac{\partial}{\partial x_i} (\rho u_i) = 0 \tag{1}$$

Momentum

$$\rho \left(\frac{\partial u_i}{\partial t} + u_j \frac{\partial u_i}{\partial x_j}\right) = - \frac{\partial p}{\partial x_i} + \rho g_i + \frac{\partial \tau_{ij}}{\partial x_j} \tag{2}$$

In equation (2) the appropriate expression for the stress tensor (τ_{ij}) is given by:

$$\tau_{ij} = \mu \left(\frac{\partial u_i}{\partial x_j} + \frac{\partial u_j}{\partial x_i}\right) \tag{3}$$

Energy

$$\rho c_p \left(\frac{\partial T}{\partial t} + u_j \frac{\partial T}{\partial x_j}\right) = \frac{\partial}{\partial x_j} \left(k \frac{\partial T}{\partial x_j}\right) + \left(\frac{\partial p}{\partial t} + u_j \frac{\partial p}{\partial x_j}\right) + \tau_{ij} \frac{\partial u_i}{\partial x_j} \tag{4}$$

The above equations, together with an equation of state for the fluid and auxiliary relations for fluid properties (μ, k and c_p), specify a system of eight equations with eight unknowns in a 2-D flow. The appropriate equation of state for our applications is the ideal gas law

$$p = \rho R^* T \tag{5}$$

where R^* is the gas constant for air in this study. Auxiliary relations for the physical properties of air are of the general form:

$$\begin{aligned} c_p &= c_p\,(T) \\ \mu &= \mu\,(T) \\ k &= k\,(T) \end{aligned} \tag{6}$$

Specific forms of the physical property relations for air which were used in this work are given by the U.S. Standard Atmosphere [17] for μ and k. c_p was fixed to a constant value taken from [18].

If, for the present flow, estimates of velocity and of the gradients of temperature and velocity can be safely drawn from the known behavior of laminar free-convection boundary layers, it is easily shown that the Rehm and Baum equations are those needed. (For details, see Appendix A3 of the report by Humphrey et al. [1]). The final equations are:

Continuity

$$\frac{\partial \rho}{\partial t} + \frac{\partial}{\partial x_i}\,(\rho u_i) = 0 \tag{1}$$

Momentum

$$\rho\left(\frac{\partial u_i}{\partial t} + u_j \frac{\partial u_i}{\partial x_j}\right) = -\frac{\partial p_d}{\partial x_i} + (\rho - \rho_\infty)\, g_i + \frac{\partial \tau_{ij}}{\partial x_j} \tag{7}$$

with τ_{ij} given by equation (3) and the dynamic component of the pressure field defined as $p_d = p - \bar{p} - \rho_\infty g_i x_i$

Energy

$$\rho c_p \left(\frac{\partial T}{\partial t} + u_j \frac{\partial T}{\partial x_j}\right) = \frac{\partial}{\partial x_j}\left(k \frac{\partial T}{\partial x_j}\right) + \frac{d\bar{p}}{dt} \tag{8}$$

In the above equations $\bar{p}$ is an average pressure in the flow domain related to ρ and T through the perfect gas law

$$\bar{p} = \rho R^* T \tag{9}$$

The above equations, like those of Boussinesq, apply to situations in which the hydrostatic variation of pressure leads to a negligible variation of density. The way in which the Boussinesq approximation arises when the driving temperature difference is small compared to the mean temperature is given by Rehm and Baum [13].

Equations (1,7,8 and 9) have been used in finite-difference form to analyze two-dimensional buoyancy-driven flows in both open and closed cavities, with the latter serving as a validation test case. The appropriate initial and boundary conditions are specified below.

Closed Cavity (See Figure 1-a)

$\bar{p}$ uniformly prescribed at t = 0.

u_i normal and tangential velocities set equal to zero at walls and prescribed at t = 0.

T prescribed at t = 0 throughout the flow domain. One side-wall was kept uniformly hot and the other uniformly cold. The top and bottom walls were kept adiabatic or with T variations prescribed.

Open Cavity (See Figure 1-b)

$\bar{p}$ uniformly constant ($\simeq$ 1 atm.)

u_i normal and tangential velocities set equal to zero at walls. Normal derivatives of u_i vanish on planes (1), (2) and (3) or specified as explained below.

T (or heat flux) prescribed at all solid walls. Temperature prescribed on plane (1), normal derivative of T vanishes on planes (2) and (3).

It should be noticed that the boundary conditions used for the open cavity calculations at planes (1), (2) and (3) are only approximate but were of sufficient accuracy for the needs of this work. That this was the case was checked by performing numerical tests in which both the positions of the boundaries relative to the cavity and the conditions set at these locations (as discussed further below) were varied. While the tests showed that the far field surrounding the cavity was sensitive to the boundary condition specifications, the flow and heat transfer characteristics within the cavity and radially around it (within about one cavity width) were not; even for cavity inclination angles of up to 45° with respect to the vertical. In practice, this set of approximated boundary conditions was successfully applied within 1.5 cavity widths of the aperture plane provided far field flow details were not required. This was possible due to the strong local determination of the flow and heat transfer characteristics within the cavity.

Nevertheless, proceeding along the lines of earlier work by Fernandez-Pello [19] an attempt was made to prescribe more realistic physical boundary conditions in order to obtain realistic predictions of the far field surrounding the cavity for a limited number of calculation cases. This was done by looking upon the

cavity as a heated horizontal line source in an infinite, initially homogeneous fluid medium. The boundary layer solution for the steady laminar plume, rising from a horizontal line source is given in, for example, Yih [20]. Thus, the streamfunction in the plume region over the line source is:

$$\psi_i = A\, X^{3/5}\, f(\eta) \tag{10}$$

where A is a constant, X is the coordinate direction vertically upwards from the line source and $f(\eta)$ is a function of the similarity variable $\eta = y/g(x)$ which tends to a finite constant value as $\eta \to \infty$. $g(x)$ is the half-width of the plume rising from the source. Since the far field flow is irrotational and solenoidal it satisfies

$$\nabla^2 \psi_o = 0 \tag{11}$$

where ψ_o is the streamfunction outside the boundary layer. Boundary conditions on ψ_o may be specified in polar coordinates (r,θ) around the line source. These are:

a) $\psi_o\,(r,\pi) = 0$; This assumes that the vertical line extending downwards from the source is a streamline.

b) $\psi_o\,(r,0) = \psi_i\,(\eta = \infty)$; This matches the inner and outer streamfunctions at the edge of the plume, ensuring that enough potential flow is entrained from the surrounding to replace the flow rising in the plume.

c) $\frac{\partial \psi_o}{\partial r}$ and $\frac{1}{r}\frac{\partial \psi_o}{\partial \theta}$ remain finite as $r \to \infty$ for $0 \leq \theta \leq \pi$.

The Laplace equation and these conditions are satisfied by the simple "separable" function

$$\psi_o = B\, r^{3/5} \sin \{3/5\, (\theta - \pi)\} \tag{12}$$

From this solution boundary conditions can be devised which imply, as they should, that the entrained flow is irrotational, and solenoidal, and that velocity components decay properly with distance from the source. This must be done without specifying the "strength", B, of the entrained flow, which is determined by processes inside the boundaries.

One possibility, which has been exploited, is to derive "radiation" conditions that are satisfied by the solution (12), no matter what the value of B. In Cartesian corrdinates (x increases vertically upwards), these conditions are

$$\frac{\partial u_x}{\partial x} = -\frac{\partial u_y}{\partial y} = -\frac{2}{5}\left(\frac{u_x x - u_y y}{x^2 + y^2}\right)$$

and (13)

$$\frac{\partial u_y}{\partial x} = \frac{\partial u_x}{\partial y} = -\frac{2}{5}\left(\frac{u_y x + u_x y}{x^2 + y^2}\right)$$

These conditions have the additional advantage, that they are invariant with respect to rotations of the coordinate axes. Thus, they can be used just as they stand for studies of inclined cavities, and they no longer insist that any particular ray, θ = constant, is a streamline.

In this work, various computations were made using equations (13) for $\partial u_x/\partial x$ and $\partial u_y/\partial x$ at plane (1), and for $\partial u_x/\partial y$ and $\partial u_y/\partial y$ at plane (2), in Figure 1-b. Boundary conditions for temperature and for the velocity at plane (3) remained the same as specified above.

THE NUMERICAL PROCEDURE

Finite Difference Equations

For purposes of deriving appropriate finite difference equations it is convenient to recast the transport equations for momentum and energy into the equivalent forms shown below:

Momentum

$$\frac{\partial \rho u_i}{\partial t} + \frac{\partial}{\partial x_j}\left(\rho u_i u_j - \mu \frac{\partial u_i}{\partial x_j}\right) = -\frac{\partial p_d}{\partial x_i} + (\rho - \rho_\infty)\, g_i + S_\rho + S_\mu \qquad (14)$$

Energy

$$\frac{\partial \rho T}{\partial t} + \frac{\partial}{\partial x_j}\left(\rho T u_j - \frac{k}{c_p}\frac{\partial T}{\partial x_j}\right) = \frac{1}{c_p}\frac{d\bar{p}}{dt} \qquad (15)$$

In the above equations the source terms are given by

$$S_\rho = \mu \frac{\partial}{\partial x_i}\left(\frac{\partial u_j}{\partial x_j}\right)$$

$$S_\mu = \frac{\partial \mu}{\partial x_j}\frac{\partial u_j}{\partial x_i} \qquad (16)$$

Equations (1, 14 and 15) may be written in the general form:

$$\frac{\partial \rho \phi}{\partial t} + \frac{\partial}{\partial x_j}\left(G_j \phi - \Gamma \frac{\partial \phi}{\partial x_j}\right) = S_\phi \qquad (17)$$

where $G_j = \rho u_j$ and, for:

$\phi = u_i$ (momentum equation recovered)

$$\Gamma = \mu$$

$$S_\phi = - \frac{\partial p_d}{\partial x_i} + (\rho - \rho_\infty) g_i + S_\rho + S_\mu$$

$\phi = T$ (energy equation recovered)

$$\Gamma = k/c_p$$

$$S_\phi = c_p^{-1} \frac{d\bar{p}}{dt}$$

$\phi = 1$ (continuity equation recovered)

$$\Gamma = S_\phi = 0$$

The general equation (17) is the basis for deriving the finite difference equations required in this work. These are obtained by volume integration of the general equation about cells surrounding nodes of the calculation mesh. The manner in which this procedure is accomplished and the rules adhered to regarding variable locations and their distributions over cell surfaces and the cell interior, have been documented in detail in various references; see for example [21]. The result for

a cell, centered about a node P is:

$$[\rho_P^n \phi_P^{n+1} - \rho_P^n \phi_P^n] \frac{\Delta v}{\Delta t} + \phi_P^{n+1} \sum A_j^{n+1} - \sum (A_j \phi_j)^{n+1} = S_\phi^{n+1} \Delta v \qquad (18)$$

Equation (18) is implicit in ϕ_P and requires the iterative solution of this variable according to:

$$(\phi_P^{**})^{n+1} = \frac{(\sum A_j^* \phi_j^*)^{n+1} + (S\phi^*)^{n+1} \Delta v + \rho_P^n \phi_P^n \frac{\Delta v}{\Delta t}}{(\sum A_j^*)^{n+1} + \rho_P^{*n+1} \frac{\Delta v}{\Delta t}} \qquad (19)$$

In the above equation Δv and Δt represent the cell volume and time step increment, respectively. The superscript n denotes time level n while the superscripts ** and * denote present and past iterations (within time step n+1), respectively. Summation is over the cell surfaces surrounding P and the A_j coefficients combine convective and diffusive contributions to the balance of ϕ.

The corresponding finite difference equation for continuity is given by:

$$(\rho_P^{n+1} - \rho_P^n) \frac{\Delta v}{\Delta t} + C_n - C_s + C_e - C_w = 0 \qquad (20)$$

where C_n, C_s ... are the mass fluxes through the north, south ... faces of the cell.

Equation (19) applies to velocities and temperature. To solve for pressure it is possible to proceed as follows[21]:

1. Velocities are written in Taylor series expansion as:

$$u_i = (u_i)^* + \left(\frac{\partial u_i}{\partial \Delta p_d}\right)^* d\Delta p_d + \left(\frac{\partial u_i}{\partial \rho}\right)^* d\rho \tag{21}$$

where ΔP is the pressure difference driving u_i. For subsonic flows of interest here:

$$u_i \simeq (u_i)^* + \left(\frac{\partial u_i}{\partial \Delta p_d}\right) d\Delta p_d . \tag{22}$$

This approximation is consistent with the neglect of high frequency pressure oscillations referred to earlier. The second term on the right-hand side of equation (22) is a velocity "correction." Thus:

$$u_i = (u_i)^* + u_i' \tag{23}$$

2. Take

$$p_d = p_d^* + p_d' \tag{24}$$

where p_d' is the "correction" sought for dynamic pressure.

3. Substitute equations (23) and (24) into the finite difference equation for continuity (20) to find:

$$(p_{d\ P}'^{**})^{n+1} = \frac{(\sum A_j'^* p_{dj}'^*)^{n+1} - (m_P^*)^{n+1} - (\rho_P^{n+1} - (\rho_P^*)^{n+1}) \frac{\Delta v}{\Delta t}}{(\sum A_j'^*)^{n+1}} \tag{25}$$

In equation (25) m_p^* is the current mass cell imbalance.

As the numerical procedure converges to the solution for n+1, $(\rho_p^*)^{n+1} \rightarrow \rho_p^{n+1}$ and the last term in equation (25) tends to zero. The neglect of this term is consistent with the assumption of a quasi-steady subsonic flow.

4. Values of p_d' are determined from equation (25) over the whole flow field and these are used to obtain final values for pressure and velocity by means of equations (24) and (23). Detailed forms of the coefficients A_j and A_j' in equations (19) and (25) are given in [21,22].

Calculation Scheme: The REBUFFS Code

The calculation scheme used to solve the finite difference equations given above originates from the TEACH-2E code developed at Imperial College (London)[23]. The modified form of the scheme developed in this study differs significantly from the parent code and was named REBUFFS: Recirculating Buoyant and Forced Flows Solver.

The REBUFFS code works according to principles similar to those embodied in the parent code. Differences arise due to the time dependent nature of the equations solved, the strong link existing between energy and momentum equations through density dependence on temperature and the use of quadratic upstream interpolation for convective differentiation. The purpose of this section is to outline the solution procedure algorithm. Much of the literature which is already available on the TEACH family of codes and related algorithms applies to the present procedure; see among others, references [21,22,23].

Once finite difference equations have been set up for all nodes in the calculation domain, within a time step they are solved iteratively by a line-by-line procedure using the tri-diagonal matrix algorithm. The dynamic component of pressure is calculated by means of the SIMPLE algorithm. The line-by-line procedure and the SIMPLE algorithm have been discussed in detail in [21].

The sequential steps taken by the calculation procedure may be summarized as follows:

1. Provide initial estimates of the values of the dependent variables (u_i, T, p_d, ρ) and the auxiliary variables, μ, k, c_p.

2. Advance in time ($t \leftarrow t + \Delta t$).

3. Advance in iterations ($n \leftarrow n + 1$).

4. Solve the momentum equations to obtain intermediate values of velocity.

5. Solve the pressure correction equation (24) to obtain p'_d.

6. Correct pressure and velocities with equations (24) and (23).

7. Solve for T.

8. Calculate ρ.

9. Calculate μ, k, c_p which, together with the new values of the dependent variables, are now used as improved estimates in Step 4.

10. Go to Step 3 and repeat 3 to 10 until a pre-established convergence criterion is satisfied.

11. Check time limits and flow steadiness. If either is attained terminate the calculations.

Miscellaneous Matters

Since the REBUFFS Code differs significantly in various aspects from the parent procedure, various miscellaneous matters arise which require clarification. These are discussed below.

i) Treatment of $\frac{d\bar{p}}{dt}$ term in the energy equation for closed cavity flow. Whereas in the case of open cavity flow geometries it follows from the definition of $\bar{p}$ that $\frac{d\bar{p}}{dt} = 0$, in a closed cavity the possibility must be allowed for $\bar{p}$ to vary with time. This is done as follows:

The perfect gas law for a cell in the calculation domain gives

$$\rho' = \frac{\bar{p}^{*}}{T^{**}} \tag{26}$$

where double and single stars denote current and previous iterative values within a time step. The total mass in the cavity is found by summing equation (26) over all cells multiplied by the respective cell volumes:

$$M' = \sum \Delta v \cdot \rho' = \bar{p}^{*} \sum \frac{\Delta v}{T^{**}} \tag{27}$$

Since total mass in the cavity is conserved (ruling out leaks), the new average pressure $\bar{p}^{**}$ must obey the relation:

$$M_o = \bar{p}^{**} \sum \frac{\Delta v}{T^{**}} \tag{28}$$

where M_o is the initial mass in the cavity. The new value of pressure is then found from equations (27) and (28) and is given by:

$$\bar{p}^{**} = \bar{p}^{*} + \frac{M_o - M'}{\sum \frac{\Delta v}{T^{**}}} \tag{29}$$

Correspondingly, the new value of density ρ^{**} at each cell is given by:

$$\rho^{**} = \frac{\bar{p}^{**}}{T^{**}} \tag{30}$$

ii) Hybrid and Quadratic Upstream Interpolation Convective Differentation

The TEACH Code, from which the present procedure evolves, employs a HYBRID (upwind/central) differencing formulation for the combined effects of convection and diffusion terms. The scheme has been documented in, for example, reference [21]. HYBRID differencing combines the accuracy of central-differencing for Peclet numbers such that $Pe \leq 2$ with the stability of upstream-differencing for $Pe > 2$. The rationale of the scheme has been explained in reference [24] and has been widely tested. The HYBRID scheme is physically more realistic at high Pe and the modifications it includes can be shown to be essential to the convergence of the iteration scheme used to solve the difference equations, as discussed in [25].

While the HYBRID differencing practice is desirable because it is inherently stable it is first order accurate and prone to numerical diffusion, particularly when flow to grid skewness arises. In order to improve the numerical accuracy of predictions performed for values of $Gr \gtrsim 10^6$ the calculation procedure was modified to embody the quadratic upstream interpolation (QUICK) scheme for convection originally proposed in [16].

In principle, the QUICK procedure avoids the stability problems of central differencing while remaining free of the inaccuracies of numerical diffusion associated with upstream (upwind) differencing. The advantage of the QUICK scheme lies in the economy of calculation storage and time cost, since it yields accurate numerical solutions on relatively coarse grids (compared to the HYBRID scheme).

The usefulness of the QUICK scheme for laminar flow regime has been documented in [26], and for laminar and turbulent flows in [27]. The

last reference provides a discussion of the various possible methods for implementing the QUICK scheme in the REBUFFS Code and should be consulted for further detail. Suffice it to remark that to retain stability and convergence properties it was necessary to split curvature terms arising from parabolic interpolation in the QUICK formulation into two groups, one of which was added to the tri-diagonal iterative matrix, the other being treated explicitly as a source term requiring re-evaluation after each sweep of the line-by-line solution algorithm within an iteration.

In this study calculations were performed using both calculation techniques. However, the QUICK scheme generally yielded grid-independent results with considerably coarser meshes than were required (for equal precision) by the HYBRID scheme. For example, calculations with QUICK on a 31 x 22 grid (in the cavity) differed by less than 0.5% with calculations on a 23 x 22 grid and by less than 1% with calculations on a 19 x 22 grid. By contrast, calculations with HYBRID on a 31 x 22 grid differed by about 4% with results computed on a 23 x 22 grid and differed (at the worst locations) by about 10% with the coarest QUICK mesh calculations. The trend in the data suggests that to obtain results as accurate as the coarsest QUICK scheme predictions with the HYDBRID scheme would require a mesh of approximately 45 x 30 nodes in the cavity. It was also verified that for conditions where unsteadiness arose in the cavity flow, time dependent characteristics were adequately resolved by the HYBRID approach. Thus, for example, the HYBRID scheme showed a steady state behavior of the flow in a square cavity with $Gr = 10^6$ and $T_w - T_\infty = 50°K$ which the QUICK scheme predicted as mildly unsteady. At $Gr = 10^7$, both schemes predicted unsteady flows but with better spatial resolution being given by the QUICK scheme. Calculations performed using the QUICK scheme on a 23 x 22 internal cavity grid distribution were considered to be sufficiently accurate for the purposes of this study.

iii) Grid Refinement and Calculation Time Considerations

The recirculating open cavity flows computed in this study required grids sufficiently refined to solve for detailed characteristics in the flows. In particular, a non-uniform grid spacing was used in the near wall regions in order to resolve adequately the boundary layer flows. Thus, at all times there were never less than four, and often as many as seven, grid nodes between the wall and the location of peak tangential velocity in the boundary layers. It should be noted that this level of grid refinement in the near wall regions was sufficient when using the QUICK scheme.

All calculations were performed on the CDC 7600 machine located in the Lawrence Berkeley Laboratory, Berkeley. Typical open cavity calculations were conducted on a 48 × 36 grid, with 23 × 22 nodes within the cavity, and required approximately 0.8 seconds per iteration. All numerical runs were started using input data derived from calculations at smaller values of Grashof number. For a given Grashof number, about 100-200 iterations were typically required to obtain a converged solution at a Grashof number one order of magnitude larger than the starting value. For equivalent grid refinement, calculations using the higher order QUICK scheme took about twice the amount of numerical run time than did calculations based on the HYBRID scheme.

Within a time step, the convergence criterion imposed in the calculation scheme was that the relative change between consecutive iterations at a monitoring point should be less than a typical value of 10^{-4} and that the residual sources of mass, energy and momentum be less than 10^{-3}. As the calculations proceeded in time the number of iterations for a converged solution within a time step decreased with time. The convergence criterion for achieving a steady state solution

was simply that the number of iterations per time step should be equal to or less than 2.

For those cases where is was known a priori that a steady state solution existed (about $Gr \leq 10^6$, depending on other conditions such as cavity aspect ratio, orientation and ΔT) is was possible to reach a converged solution within a single time step by setting the time step to a very large number. It was verified that significant differences did not exist between steady state solutions reached through either one of the above approaches.

Validation

The elliptic numerical procedure was validated by reference to two fundamental test cases: the heated semi-infinite vertical flat plate and thermally driven flow in a two-dimensional enclosure with hot and cold (vertical) side walls. Comparison data for the first test case were taken from the theoretical work of Ostrach [28] which includes experimental results of others. Corresponding data for the enclosure flow were taken from the detailed experimental study recently performed by Duxbury [29]. Duxbury's data is particularly attractive for evaluation purposed since it includes temperature ranges for which departures from the Boussinesq approximation may be expected to arise. A complete discussion of the test case calculations has been given in the report by Humphrey et al [1]. A summary of those findings is provided here.

Vertical flat plate laminar flow calculations were performed for a plate of length L such that $Gr_{x|x=L} = 10^7$, with $T_W - T_\infty = 20°K$. The boundary conditions for this flow correspond to the special case indicated in Figure 1-b. Calculations were performed using the HYBRID and QUICK schemes respectively. Grid independent results in excellent agreement with Ostrach's solution

were obtained with the QUICK scheme on a grid which had 40 nodes in the main flow direction and 30 nodes transverse to the flow. The width of the calculation domain was taken as twice the boundary layer thickness at the furthest downstream location, corresponding to x = L. Although the grid was uniformly spaced it allowed for not less than 4 calculation nodes between the wall and the location of maximum velocity at any stream-wise location. By contrast, the HYBRID scheme did not yield grid independent results on the same grid due to the lack of sufficient near-wall nodes, required by this lower order accuracy scheme.

Thermally driven enclosure flow calculations corresponding to Duxbury's study were carried out by specifying experimentally determined boundary conditions for temperature in the numerical procedure. In his work Duxbury maintained the side walls of the enclosure at constant uniform known values of temperature and, because the top and bottom walls of the enclosure were not truly adiabatic, measurements of temperature at those locations were also made. The boundary conditions for this flow are illustrated in Fig. 1-a.

Typical temperature and Nusselt number calculations and their comparison with Duxbury's data are presented for an aspect ratio of 0.8 in Figs. 2-a and b. Comparisons for other aspect ratios and flow conditions were also carried out and showed similar levels of agreement. Especially noteworthy is the fact that detailed cross-over features of temperature profiles corresponding to a cavity aspect ratio a/b = 1.6 were accurately predicted by the calculation scheme. In the calculations Ra was 4×10^6 and $T_H - T_C = 60°K$ (the largest ΔT investigated in Duxbury's work) and significant departures from the Boussinesq approximation were observed. While calculated temperature profiles always showed very good qualitative agreement with the measurements discrepancies of up to 10% between measurements and calculations were observed. In general, calculated temperatures were always higher than their corresponding

experimental values. This is explained, in part, by the observation made by Duxbury that end wall losses in the experiment were as large as 30% of the total heat input.

Velocity profiles have not been plotted, simply because there is no data for their relative comparison. However, from the calculations it was possible to derive velocity vector fields and streamfunction plots. These were in excellent qualitative agreement with the flow visualization photographs provided by Duxbury.

In addition to the above comparisons, other calculations were performed to show the effect of side wall temperature difference and Rayleigh number on the value of mean pressure within a sealed enclosure. The results of these calculations are shown in Fig. 2-c where a relative comparison is made with similar calculations by Leonardi and Reizes [11], although for slightly different conditions. The calculations of Leonardi and Reizes correspond to values of $2(T_H - T_C)/(T_H + T_C) = 0.4$ and 0.8 whereas present calculations are for a value of this parameter equal to 0.67. The complex variation of mean pressure indicated in Fig. 2-c is an indirect reflection of fluid medium physical property variations with temperature* and comes as a consequence of the complicated balance struck between the modes of energy storage within the enclosure (kinetic, potential and internal). A more detailed discussion of this effect may be found in the paper by Leonardi and Reizes.

---

* μ was given by Sutherland's law and k was found by holding Pr and c_p constant. This approximation, over the temperature range of the calculations ($300\ K \lesssim T \lesssim 550\ K$), was quite adequate.

OPEN CAVITY RESULTS AND DISCUSSION

General Considerations

The numerical results of calculations performed for air in an open cavity geometry are presented and discussed in this section. The variables of interest in the calculations were: Grashof number (Gr), the difference between cavity wall and ambient temperature ($\Delta T = T_w - T_\infty$), cavity aspect ratio (a/b) and angle of inclination (α).

As shown in Fig. 1-b the cavity is connected at the aperture plane to adiabatic upstream and downstream flat plate sections which allows an unambiguous determination of the flow in the vicinity of the entrance and exit corner regions. All three internal walls in the cavity were kept at the same temperature, T_w. Since $\Delta T/T_\infty$ is an independent parameter in the non-Boussinesq form of the conservation equations governing the flow, two levels of temperature were calculated corresponding to values of $\Delta T = 50°K$ and 500°K, respectively. The ambient temperature, T_∞, was set equal to 288°K for all calculations.

Calculations were performed for values of Grashof equal to 10^4, 10^5, 10^6, 10^7 and 3×10^7. In general, Grashof number was varied by changing the reference length corresponding to the aperture plane dimension (b) shown in Fig. 1-b while holding $\Delta T/T_\infty$ fixed. Although the bulk of the calculations were performed for a cavity of square cross-section with inclination angle of zero degrees, flows with aspect ratios a/b = 1/2 and 2 (with $\alpha = 0°$) and a/b = 1 (with $\alpha = 20°$ and 45°) were also computed. All the results presented in this section were obtained using the QUICK higher order convective scheme.

A note is in order regarding the calculations performed for $\alpha = 45°$. For this case the numerical scheme converged very slowly due to the larger under-relaxation imposed on pressure, velocity and temperature to ensure stability. In order to obtain numerical results in a reasonable (affordable) amount of computer time the convergence criterion was increased from 10^{-4} to 10^{-3}. By necessity then, these results are less accurate and comparisons with the remaining cases, although valuable, should be made with this restriction in mind.

Prior to discussing in detail the specific dependence of thermally driven cavity flow on the parameters mentioned above, various features of the flow are presented first in order to provide some insight regarding its general characteristics. Figure 3-a shows a typical steady state vector velocity field in and about a vertically oriented cavity of square cross-section for conditions of $Gr = 10^5$ and $\Delta T = 50°K$. The degree of grid refinement (48 × 36 nodes, with 23 × 20 inside the cavity) and the relative distribution of grid nodes, which were unequally spaced in the near wall zones to resolve the boundary layer flow, is illustrated by the velocity vector positions in the figure*. A magnified view of the corresponding temperature field within the cavity is shown in Fig. 3-b. These calculations were performed using the improved far-field boundary condition treatment leading to equations (13). The vector field of Fig. 3-a shows cold fluid entering the cavity over the bottom 2/3 of the aperture plane. Hot fluid leaving the cavity emerges from the top 1/3 of the aperture plane. Intense shearing of the flow arises at the horizontal plane in the cavity where the entering and emerging flow fields meet. By contrast with the entering flow, which is drawn almost radially from the surroundings, the flow emerging from the cavity is quickly deflected vertically upwards by buoyant forces. The air heated in the cavity, particularly at the vertical back wall, drives the flow and is the cause for a substantial amount of entrainment from the surrounding fluid medium, especially along horizontal planes above the cavity. For the calculation conditions in Fig. 3 recirculation regions did not arise in the

*The near-wall grid positions for velocity are too closely spaced to be clearly discerned in the figure.

cavity. Temperature contours shown in Fig. 3-b and detailed velocity distributions (not shown here) attest to the boundary layer nature of the flow, especially at the bottom wall.

For values of Grashof $\gtrsim 10^7$ the flow field became noticeably unsteady, giving rise to localized recirculation zones on the bottom wall in the cavity. The nature of the unsteady flow was periodic and is illustrated in Figs. 4 and 5 for Gr = 3×10^7 at consecutive times within a cycle, 2 seconds apart. The figures show small recirculating flow regions or eddies being convected along the cavity bottom wall, and vertically upwards along the back wall. As these "heat bubbles" move, diffusion effects gradually smear out their thermal identifies. At the later instant in time, the velocity vector plot shows a small eddy rising along the back wall as a result of the wave-like disturbance traveling downstream. The recirculating flow region in the top half of the *aperture plane* was also a periodic feature of the flow for the conditions calculated and is related to the eddy shedding process occurring on the back and bottom walls. Thus, vorticity is fed into the aperture plane by the bottom wall eddies and is the cause for a small amount of periodic thickening of the thermal layer at the top wall in the cavity. The same effect was not observed for inclination angles of α = 20° and 45° and may be due to having taken larger time steps (2s as opposed to 0.1s) to hasten convergence. However, the flow is stabilized by inclining the cavity and detailed (but costly) calculations will be required to settle the question of the presence of a periodic recirculating zone in the aperture plane for $\alpha > 0°$. Although it appears to originate at the edge of the cavity bottom wall, the flow unsteadiness was definitely thermal in nature since equivalent calculations with an adiabatic bottom wall did not produce the eddy structures. A similar unsteadiness to the one just discussed was also observed for the flow

in a cavity with a/b = 2, $\alpha = 0°$, $Gr = 10^7$ and $\Delta T = 500°K$. However, for the same conditions but in a cavity with a/b = 1/2 the unsteadiness was less, suggesting a stabilizing effect of decreasing cavity aspect ratio on the flow. Flow visualization results presented in [30] confirm the existence of the bottom wall eddies for thermally-driven air flow in a cavity with a/b = 1 and $\alpha = 0°$. In the experiment, $\Delta T \simeq 90°C$ and $Gr \simeq 6 \times 10^6$ with an ambient temperature, $T_\infty = 20°C$. The eddies in [30] were generated and driven along the bottom cavity wall at a frequency of approximately 1-2 Hz. This compares favorably with the frequency of approximately 0.5 Hz displayed by the calculations discussed above.

In addition to the above, calculations were performed for a square cavity inclined at angles of $\alpha = 20°$ and $\alpha = 45°$ with respect to gravity. It was verified that for both inclination angles, the flow within the cavity and in the aperture plane was fairly insensitive to large perturbations falsely introduced at the far field boundaries. This confirmed the notion that the boundaries were sufficiently removed from the cavity so as not to influence significantly the flow field within it. A comparison between Figs. 6 and 7 illustrates the effect of increasing Grashof number from 10^5 to 10^6 for a fixed inclination angle of $\alpha = 20°$ and $\Delta T = 50°K$. While both cases show a large recirculation zone within the cavity, the larger Grashof number case reveals a second smaller, *quasi-steady* recirculating flow region in contact with the cavity top wall. The steadiness of the high Grashof number flow is in contrast to that calculated in a cavity of identical conditions but with $\alpha = 0°$, in which a weak but observable unsteadiness was found. The stabilizing effect of an inclined geometry was further confirmed for the case of a cavity flow with $\alpha = 45°$, $Gr = 10^6$ and $\Delta T = 50°K$ shown in Figs. 8.

The relatively strong influence of cavity orientation on the flow is readily

apparent and is manifested by the enlarged recirculating zone appearing at the top wall. For this case, all walls in the cavity behave as inclined flat plates and, in conjunction, act to create a complex doubly recirculating flow pattern within the cavity. A similar cavity flow field has been predicted by Humphrey and Jacobs [31]. However, in their case the top wall recirculation zone was driven by free stream forced convection. Particularly noticeable in the present case is the fact that cold flow entering the cavity aperture plane must be strongly deflected in order to proceed along the bottom wall to the back wall. Temperature contours in Fig. 8b show a region of hot fluid trapped in the top inner corner of the cavity and reflect a condition of stable stratification within the cavity.

Velocity and Temperature Profiles

While the results presented in the previous section are very descriptive of the flow, for quantitative purposes, and particularly for comparison with other works, it is useful to provide detailed profiles of calculated velocity and temperature distributions. Figures 9 to 11 show dimensionless velocity and temperature profiles at three x/b and four y/a locations in a cavity of square cross-section for two values of Grashof number, ΔT and α, respectively. In each figure the velocity profiles have been normalized with respect to the maximum value of u_y in the aperture plane, $u_{y_{max}}$, which is also given.

For $\alpha = 0°$, the velocity profiles show a decreasing boundary layer thickness and a displacement of velocity maxima towards their respective walls as Grashof increases. Correspondingly, the u_y profiles at the aperture plane ($y/a = 1.0$) become more uniform in the flow region penetrating the cavity. The uniform entrance profile occupies about 2/3 of the cavity aperture plane for $Gr = 10^4$, increasing to a value of about 3/4 of b for $Gr = 10^6$ and 10^7. The u_y velocity profiles show local maxima in the entry flow region, at the bottom wall of the cavity. Similarly, the u_x profiles show corresponding but larger maxima in the back wall region of the flow (near $y/a = 0$). It would appear that the local acceleration of the flow on both walls is due to the contribution of buoyant forces to the momentum balance in the cavity. From a relative comparison of the temperature profiles, it is readily seen that the depth of penetration of cold flow into the cavity increases with Grashof number.

Superimposed on Fig. 9-a and b are velocity and temperature profiles corresponding to a $\Delta T = 500°K$ for the same Grashof number. This higher temperature flow exits the cavity at a maximum velocity of 0.23 m/s which

is twice as large as that corresponding to the lower temperature flow ($\Delta T = 50°K$). The higher temperature flow also shows a larger portion of the aperture dedicated to entering fluid, as well as a less uniform entrance velocity profile at this location. Considerable thickening of the boundary-layer occurs at the back wall of the cavity for $\Delta T = 500°K$. Corresponding temperature contours show the same effect, with a larger proportion of the fluid in the cavity being heated by the walls.

Velocity and temperature profiles corresponding to a cavity inclination angle $\alpha = 45°$ (see Figs. 8a and b) are given in Figs. 11a and b. A comparison between Figs. 10 and 11 shows that the effect of inclining the cavity has been to accelerate three-fold the peak velocity of fluid flowing along the bottom wall in the cavity. However, the peak value of velocity of the fluid leaving the cavity through the aperture plane is substantially smaller. The presence of thermal stratification for this cavity inclination is evidenced clearly in the temperature profiles corresponding to back and top wall locations. As would be expected, corresponding results for $\alpha = 0°$ do not show this strong influence on the flow.

Heat Transfer Calculations

Nusselt number calculations were performed at the cavity walls by evaluating numerically the expression:

$$Nu_w = \frac{b}{(T_w - T_\infty)} \left.\frac{\partial T}{\partial n}\right|_w \qquad (31)$$

In the expression, n denotes the normal to any wall and b is the cavity aperture plane length, used as a reference.

Figure 12 provides a comparison conducted with the Boussinesq approximated data available in Penot [3] for Grashof numbers of 8×10^4 and 8×10^5 respectively for a/b = 1, $\alpha = 0°$ and $\Delta T = 50°K$. For $Gr = 8 \times 10^4$, qualitative agreement between the results is quite good although quantitative differences appear. For $Gr = 8 \times 10^5$ present results for Nu differ significanlty from those given by Penot. In particular, the results of this study show smaller values of Nu at the bottom wall of the cavity. At the top wall, values of Nu are comparable except near the top inner corner where a maximum appears in the present work. The differences are explained, in part, by the relative coarseness of the calculation grid used by Penot in his numerical scheme, which was 12 x 12 in the cavity. Also included in Fig. 12 are calculations obtained using the HYBRID and QUICK scheme respectively. These results show that differences between the schemes become significant for $Gr \gtrsim 10^6$. Similarly to Penot, present calculations for $Gr = 10^7$ exhibited a localized minimum in the Nusselt number halfway along the bottom wall of the cavity. The minimum in Nu corresponds to a swell in the bottom wall boundary layer which eventually leads to the formation of the small recirculation zones discussed earlier.

Although they are not shown here, Nusselt number calculations along the bottom wall reflected the presence of the recirculation zones

for $Gr = 3 \times 10^7$. For a cavity inclination of $\alpha = 45°$, the calculations indicated that stable thermal stratification within the cavity and the absence of unsteadiness prevented the occurrence of local maximum and minimum values of Nu at the top and bottom wall, respectively.

A summary of the heat transfer predictions is presented in Table 1 for various conditions of interest. The results show that, in general, Nusselt number increased with increasing Grashof number and decreasing aspect ratio. The influence of cavity orientation on heat transfer from the separate cavity walls is more complex. Thus, with increasing α, Nusselt number on the bottom wall increases while Nusselt number on the back wall decreases. This is explained by the fact that with increasing α the back plate departs from its vertical orientation towards an inclined (downward facing) orientation while the bottom plate goes from a horizontal orientation towards an inclined (upward facing) orientation. The net effect is to enhance heat transfer from the bottom wall while reducing that from the back. The top wall in the cavity shows decreasing Nusselt for Grashof = 10^6 corresponding to the appearance and growth of a recirculation zone at this wall with increasing α (see Figures 7 and 8).

Temperature effects on heat transfer for cavities of equal size are illustrated by comparing values of Nu in the table corresponding to $Gr = 10^4$, $\Delta T = 50°K$ with $Gr = 10^5$, $\Delta T = 500°K$ and values of $Gr = 10^6$, $\Delta T = 50°K$ with $Gr = 10^7$, $\Delta T = 500°K$. In both cases the heat transfer from the top wall in the cavity increases with an increase in ΔT. This is due to the back-wall jet-like behavior of the flow which, when impinging against the top wall, readily removes heat by convection. By contrast, the bottom wall shows a decrease in heat transfer with an increase in ΔT. A detailed comparison

between velocity and temperature profiles at the bottom wall of the cavity revealed that the fluid heated along this wall is deflected into the cavity core sooner at lower Grashof numbers. It appears that fluid elements near the bottom wall have a longer residence *length* in this region for the higher Grashof number. Thus, although initial heat transfer to the fluid elements is high, since they are forced to remain near the bottom wall as they are convected by the flow, their capacity to remove heat from the wall is diminished. The net effect is for a reduction in total heat transfer from this wall.

CONCLUSIONS

A two-dimensional, elliptic, transient, numerical calculation procedure firmly based on the formal analysis of Rehm and Baum [13] has been developed, tested and subsequently applied to the case of thermally-driven laminar flow in cavities of rectangular cross-section. The nature of the equations solved is such that high-frequency pressure fluctuations (and the time-step limitations they impose) are eliminated from the calculations while relatively large temperature and density variations are accounted for. The Boussinesq approximation is dispensed with and density variations are found directly from solutions for the temperature and pressure fields in conjunction with the perfect gas equation of state. For open cavity flows density varies with temperature only since pressure is a prescribed constant in the equation of state.

The present method makes use of the QUICK quadratic upstream interpolation technique for finite differencing of convective terms in the transport equations. In this way, numerical diffusion associated with straightforward upwind differencing (as employed in the HYBRID scheme) is reduced for $Gr \gtrsim 10^6$, particularly when flow-to-grid skewness arises. The numerical method is embodied in a computer code (REBUFFS) which solves for primitive variables on an interconnected staggered grid configuration according to a well established guess-and-correct iterative procedure. The method can readily be extended to predict transient three-dimensional flows in orthogonal coordinates.

New numerical results are reported for the thermally-driven laminar flow of air in open cavities of rectangular cross-section. It has been found that the flow field approaching the cavity is a function of the far-field boundary condition specification. Realistic conditions can be formulated which ensure that the flow entrained through the far field is rotational and solenoidal. Notwithstanding, calculations show that the flow field *within*

the cavity and in the aperture plane is determined mainly by local heat transfer effects and is relatively insensitive to the far-field specifications provided the far-field boundary is located at a distance of 1.5 cavity heights or more from the aperture plane.

Inspection of the predictions shows that flow unsteadiness similar to that observed in [30] arises for values of $Gr > 10^6$ for $a/b = 1$ and $\alpha = 0°$. The unsteadiness appears as a sequence of recirculating eddies or "hot spots" which originate at the edge of the cavity bottom wall along which they are made to flow towards the cavity back wall where they rise. Changes in cavity orientation produce striking variations in cavity flow patterns due to the interchanging heat transfer roles of the walls as the cavity is inclined. The calculations presented here for $\alpha = 20°$ and $45°$ show clearly that thermal losses diminish with increased values of the inclination angle α due to stable stratification of the flow and decreased unsteadiness. For $Gr \gtrsim 10^7$ and for values of $\alpha = 20°$ and $45°$ strong under-relaxation of the calculation variables was required to retain numerical stability. Unfortunately, this practice reduces the rate of convergence of the calculation scheme and makes it costly to use.

The effect of increasing $T_w - T_\infty$ in thermally driven cavity flow is to enhance heat losses from the top wall while reducing corresponding losses from the bottom wall. The latter effect is explained by the reduced capacity of fluid elements to remove heat from the bottom wall in the cavity where they are constrained to remain by the external flow while their temperature increases. Finally, the average Nusselt number is seen to increase with increasing Gr number while it decreases with increasing aspect ratio, as would be anticipated.

ACKNOWLEDGEMENTS

We would like to express our sincere thanks to M. Abrams, R. Gallagher, J. Kraabel and S. Paolucci of Sandia Laboratories for frequent and helpful discussions relating to this work. We are especially grateful to T. Han and W-M To of the Mechanical Engineering Department, University of California, Berkeley for their most valuable assistance in the testing of the calculation code. This study was made possible through Sandia National Laboratories Research Contract No. 20-1012. The authors are glad of this opportunity to express their appreciation for the financial support.

REFERENCES

1. J.A.C. Humphrey, F.S. Sherman, P. LeQuere and K. Chen, "Investigation of Free-Forced Convection Flows in Cavity-Type Receivers," Mid-Term Report to Sandia National Laboratories, Livermore, CA. 94550, July 1980.

2. D.L. Siebers, M. Abrams and R.J. Gallagher, "Solar Thermal Central Receiver Systems," Paper 79-WA/HT-38 presented at the 1979 Winter Annual Meeting of the ASME, New York, N.Y.

3. F. Penot, "Transfert de chaleur par convection naturelle dans une cavite rectangulaire isotherme ouverte sur une face," Revue Phys. Appl. 15, pp. 207-212, 1980.

4. P. Orlandi, M. Onofri, and F. Subetta, "Interaction between Natural and Forced Convection in a Complex Geometry," Proc. of Heat Trans. and Fluid Mech. Institute, 1978.

5. A. Rubel and F. Landis, "Laminar Natural Convection in a Rectangular Enclosure with Moderately Large Temperature Difference," Heat Transfer, Vol. 4, NC 2-10, 1970.

6. V.I. Polezhaev, "Numerical Solution of the System of 2-D Unsteady Navier Stokes Equations for a Compressible Gas in a Closed Region," Fluid Dynamics, Vol. 2, pp. 70-74, 1967.

7. L.W. Spradley and S.W. Churchill, "Pressure and Buoyancy Thermal Convection in a Rectangular Enclosure," J. Fluid Mechanics, Vol. 70, Part 4, pp. 705-720, 1975.

8. P. LeQuere and T. Alziary de Roquefort, "Three Dimensional Numerical Evaluation of the Heat Loss through Natural Convection in a Solar Boiler," 3rd GAMM Conference on Numerical Methods in Fluid Mechanics, DFVLR, Cologne, West Germany, October 1979.

9. W.A. Briley and H. McDonald, "Solution of the Multidimensional Compressible Navier-Stokes Equations by a Generalized Implicit Method," J. Computational Physics, Vol. 24, p. 372, 1977.

10. J. Douglas and J.E. Gu-n, "A General Formulation of Alternating Direction Implicit Methods," Numerische Mathematik, Vol. 6, pp. 428-453, 1964.

11. E. Leonardi and J.A. Reizes, "Natural Convection in Compressible Fluids with Variable Properties," Numerical Methods in Thermal Problems, (ed. R.W. Lewis and K. Morgan) Proc. of the 1st International Conference, Univ. College Swansea, 1979. Pineridge Press.

12. G.D. Mallinson and G. deVahlDavis, 3-Dimensional Natural Convection in a Box: A Numerical Study. J. Fluid Mechanics, Vol. 83, Part 1, pp. 1-31, 1977.

REFERENCES (cont.)

13. R.G. Rehm and H.R. Baum, "The Equations of Motion for Thermally Driven, Buoyant Flows", Journal of Research of the National Bureau of Standards, 83, No. 3, pp. 297-308, 1978.

14. C.K. Forester and A.F. Emery, "A Computational Method for Low Mach Number Unsteady Compressible Free Convective Flows", J. Computational Physics, 10, 487-502, 1972.

15. A.C. Ku, M.L. Doria and J.R. Lloyd, "Numerical Modeling of Unsteady Buoyant Flows Generated by Fire in a Corridor", 16th Symp. (Intl.) on Combustion, CI., pp. 1373-1384, 1976.

16. B.P. Leonard, "A Stable and Accurate Convective Modeling Procedure Based on Quadratic Upstream Interpolation", Comp. Meths. Appl. Mech. Eng., 19, p. 59, 1979.

17. U.S. Standard Atmosphere, National Oceanic and Atmospheric Administration, National Aeronautics and Space Administration, United States Air Force, Washington, D.C., October 1976.

18. O.A. Hougen, K.M. Watson and R.H. Ragatz, "Chemical Process Principles", Part 1, p. 255, 2nd edition, 7th printing, John Wiley and Sons, Inc., New York, 1964.

19. A. Fernandez-Pello and F.A. Williams, "A Theory of Laminar Flame Spread Over Flat Surfaces of Solid Combustibles", Combustion and Flame, 28, pp. 251-277, 1977.

20. C-S Yih, "Fluid Mechanics", McGraw-Hill, Inc., New York, 1969.

21. S.V. Patankar, "Numerical Heat Transfer", McGraw-Hill Book Company, New York, 1980.

22. J.A.C. Humphrey, "Numerical Calculations of Developing Laminar Flow in Pipes of Arbitrary Curvature Radius", Can. J. Chem. Eng.,56, pp. 151-164, 1978.

23. A.D. Gosman and W.M. Pun, Lecture Notes for Course Entitled, "Calculation of Recirculating Flows", Imperial College HT5/74/2, 1974.

24. D.B. Spalding, "A Novel Finite-Difference Formulation for Differential Expressions Involving both First and Second Derivatives", Int. J. Num. Methods. Eng., 4, p. 551, 1972.

25. S.V. Patankar, Numerical Prediction of Three-Dimensional Flows, in B.E. Launder (ed.), Studies in Convection: Theory, Measurements and Applications, Vol. 1, Academic, New York, 1975.

26. M.A. Leschziner, "Practical Evaluation of Three Finite-Difference Schemes for the Computation of Steady-State Recirculating Flows", Comp. Meths. in Appl. Mech. Eng., 1980.

REFERENCES (cont.)

27. T. Han, J.A.C. Humphrey and B.E. Launder, "A Comparison of Hybrid and Quadratic-Upstream Differencing in High Reynolds Number Elliptic Flows", Comp. Meths. in Appl. Mech. Eng., 1981.

28. S. Ostrach, "An Analysis of Laminar Free-Convection Flow and Heat Transfer about a Flat Plate Parallel to the Direction of the Generating Body Force", NACA TR 1111, 1953.

29. D. Duxbury, U.K., "An Interferometer Study of Natural Convection in Enclosed Plane Air Layers with Complete and Partial Vertical Divisions", Ph.D. Thesis, University of Salford, 1979.

30. J.A.C. Humphrey, L. Miller and K.S. Chen, "Experimental Investigation of Thermally Driven Flow in Open Cavities of Rectangular Cross-Section," Journal of Heat Transfer, Trans. ASME, 1981.

31. J.A.C. Humphrey and E.W. Jacobs, "Free-Forced Laminar Flow Convective Heat Transfer from a Square Cavity in a Channel with Variable Inclination," Int. Journal of Heat and Mass Transfer, 1981.

Table 1: Average $\overline{Nu}^{+}$ on each cavity wall as a function of relevant parameters

			a/b = 1		
			α		
		ΔT (°K)	0°	20°	45°
Gr	10^4	50	1.16 (TOP WALL)		
			0.725 (BACK WALL)		
			3.02 (BOTTOM WALL)		
		500	0.640		
			0.103		
			1.09		
	10^5	50	2.79	1.73	
			2.74	2.25	
			5.22	5.86	
		500	1.23		
			0.602		
			2.59		
	10^6	50	5.09	2.56	1.75
			6.29	5.18	2.12
			8.39	10.30	10.97
	10^{7*}	50	9.05		
			17.66		
			21.53		
		500	6.06		
			6.31		
			7.85		
3	10^{7*}	50	12.23		
			24.12		
			28.92		

	α = 0°	
	a/b	
	2	0.5
	3.43	6.97
	4.65	7.22
	6.10	9.98

$$\overline{Nu}^{+} = \frac{1}{\ell_{wall}} \int_{0}^{\ell_{wall}} \frac{b(\partial T/\partial n)}{(T_w - T_\infty)} \, d\ell$$

* Instantaneous values

Table 2: Conductive plus convective thermal losses across aperture plane

b(m)	Gr ($\Delta T = 50°K$, a/b = 1)	w/m^2 α 0°	20°	45°
$1.045\ 10^{-2}$	10^4	666		
$2.25\ 10^{-2}$	10^5	681	621	
$4.85\ 10^{-2}$	10^6	582	530	428
$1.50\ 10^{-1}$	$3\ 10^7$ *	496		

* Instantaneous values

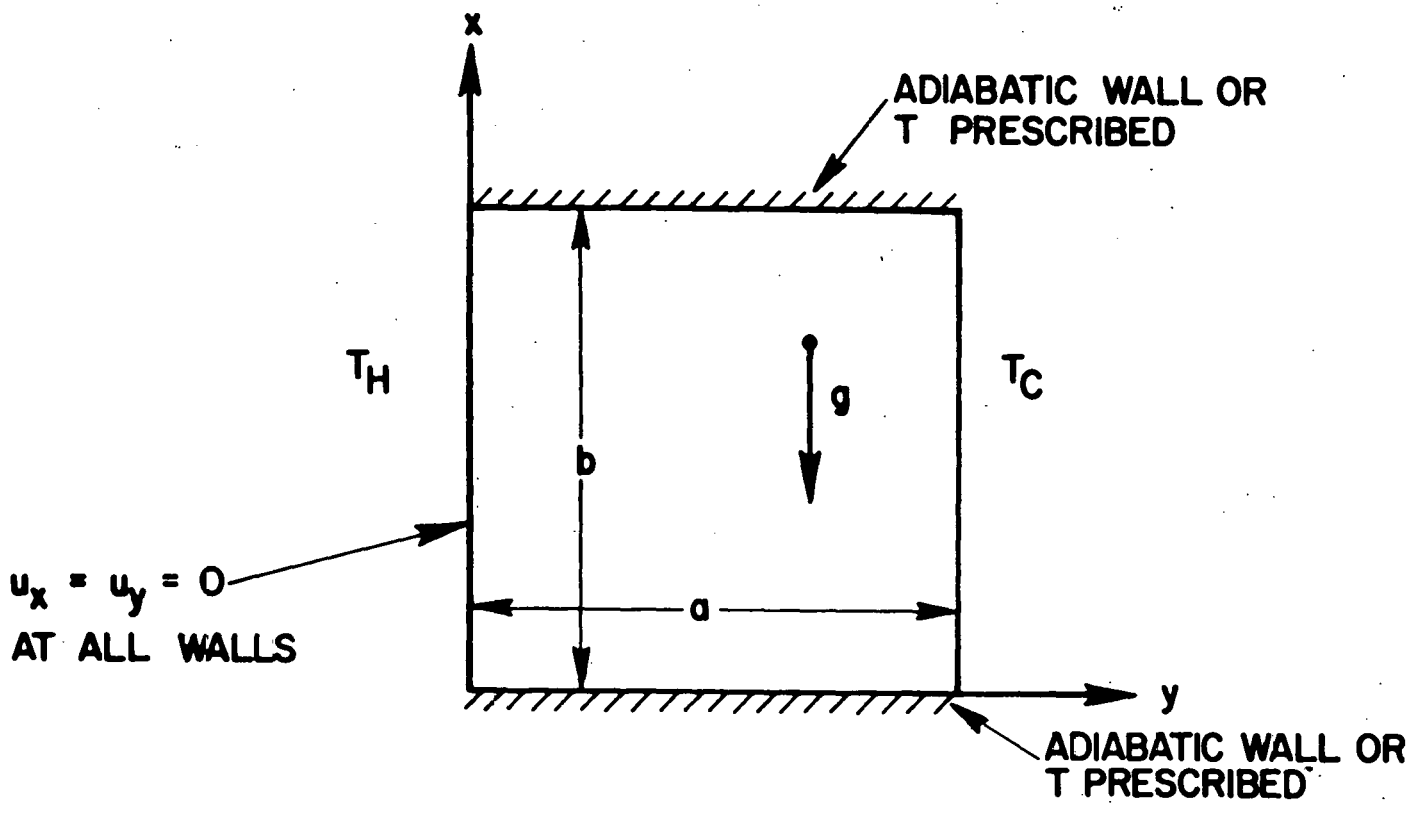

Fig. 1-a Closed cavity geometry and boundary conditions.

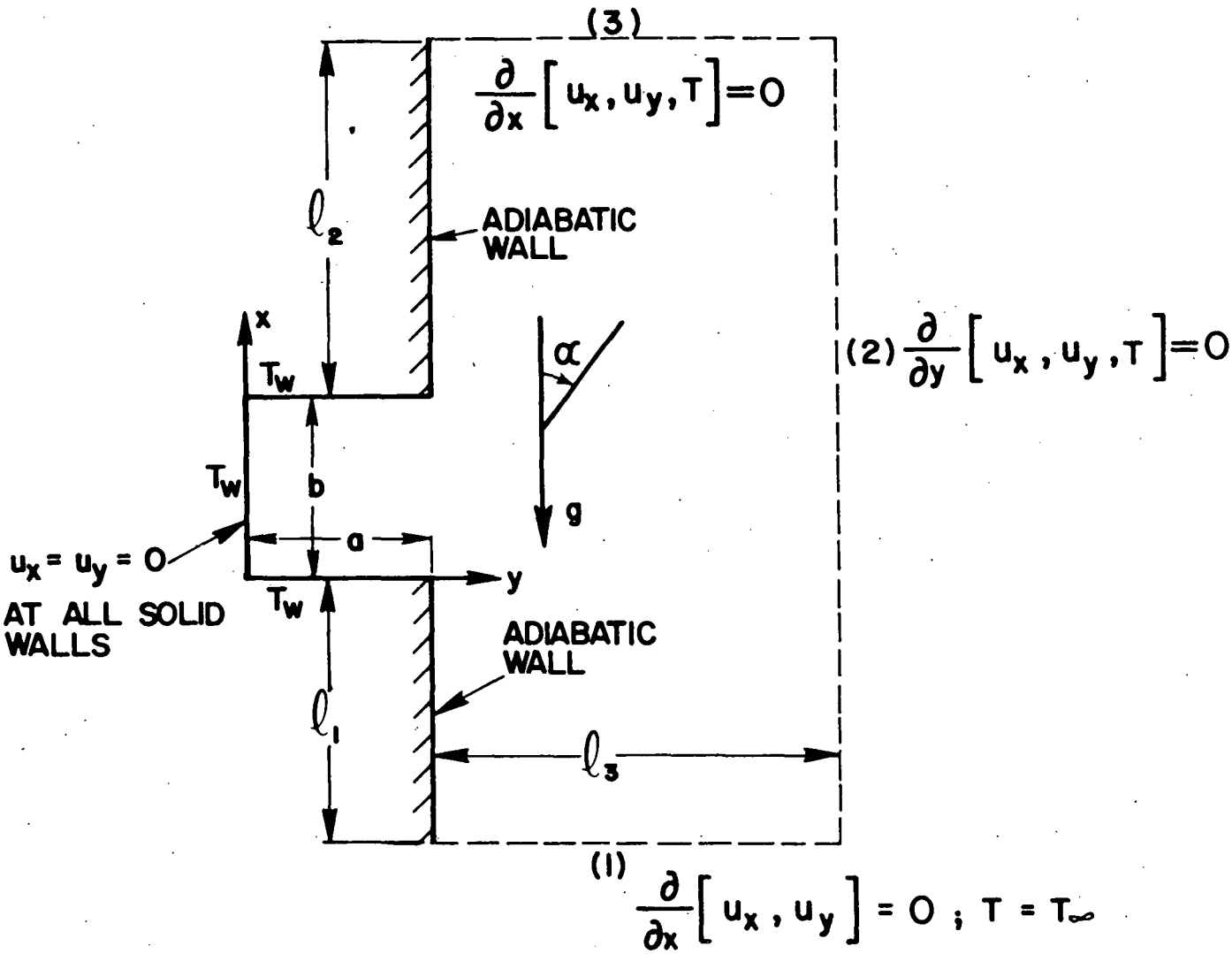

Fig. 1-b Open cavity geometry and boundary conditions. In the calculations ℓ_1 = b, ℓ_2 = 1.5 b, ℓ_3 = 2 b. Special case of vertical flat plate is obtained by setting a = 0. Far-field boundary conditions at planes (1) and (2) corresponding to equations (13) also calculated.

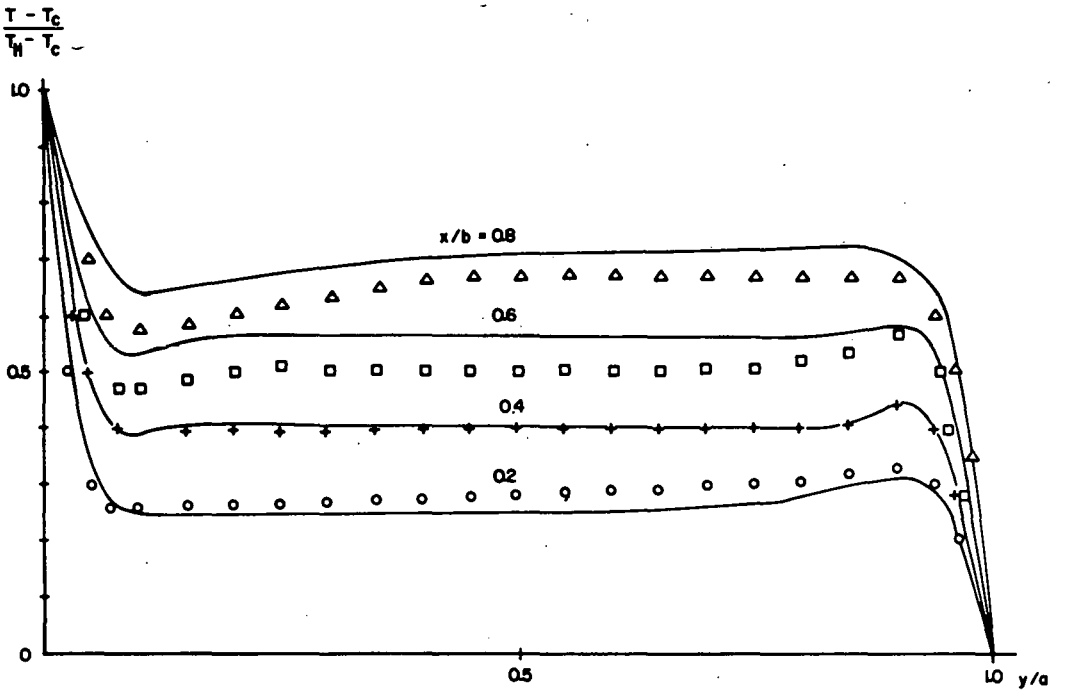

(a)

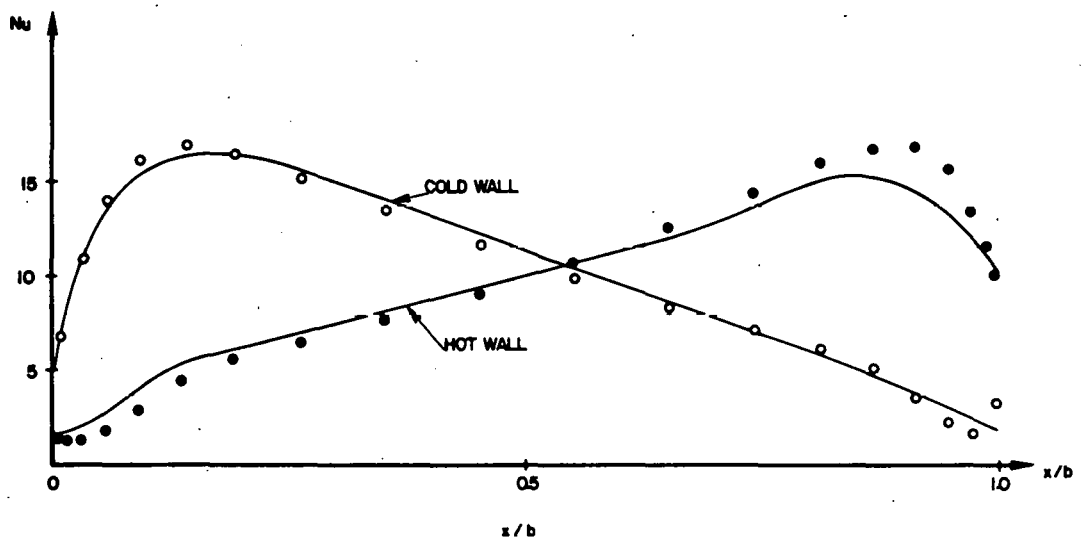

(b)

Fig. 2 Relative comparison of calculated and measured temperature (a) and side-wall Nusselt number (b) distributions in a thermally driven enclosure of aspect ratio a/b = 0.8 with $Ra = 4 \times 10^6$ and $\Delta T = 60°K$. Experimental data from Duxbury (shown as points).

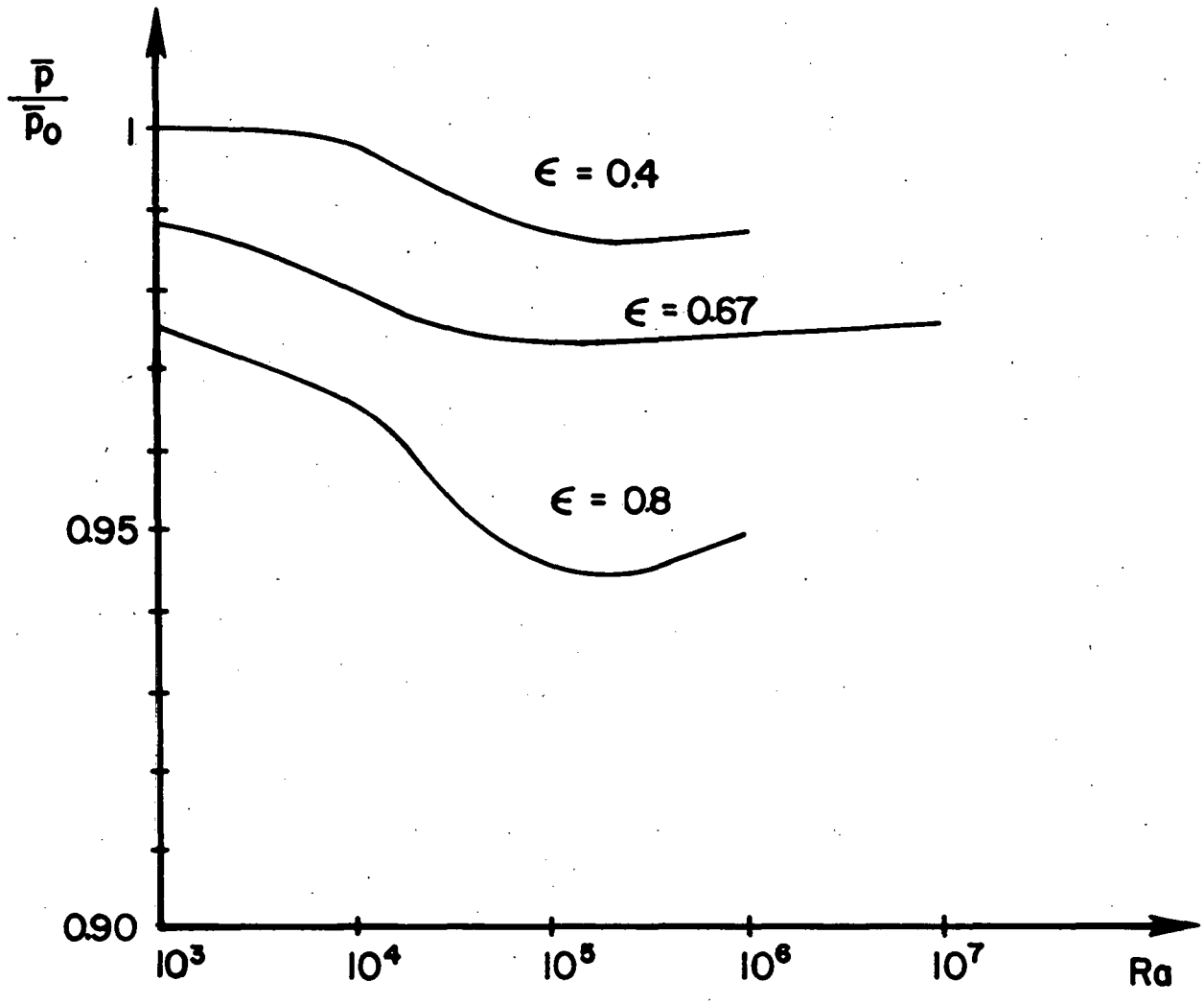

Fig. 2-c Average pressure variation in a thermally driven enclosure flow as a function of Ra number and $\varepsilon = 2\Delta T/(T_H + T_C)$. Results for $\varepsilon = 0.4$ and 0.8 are from Leonardi and Reizes [11]; $\varepsilon = 0.67$ values correspond to this work.

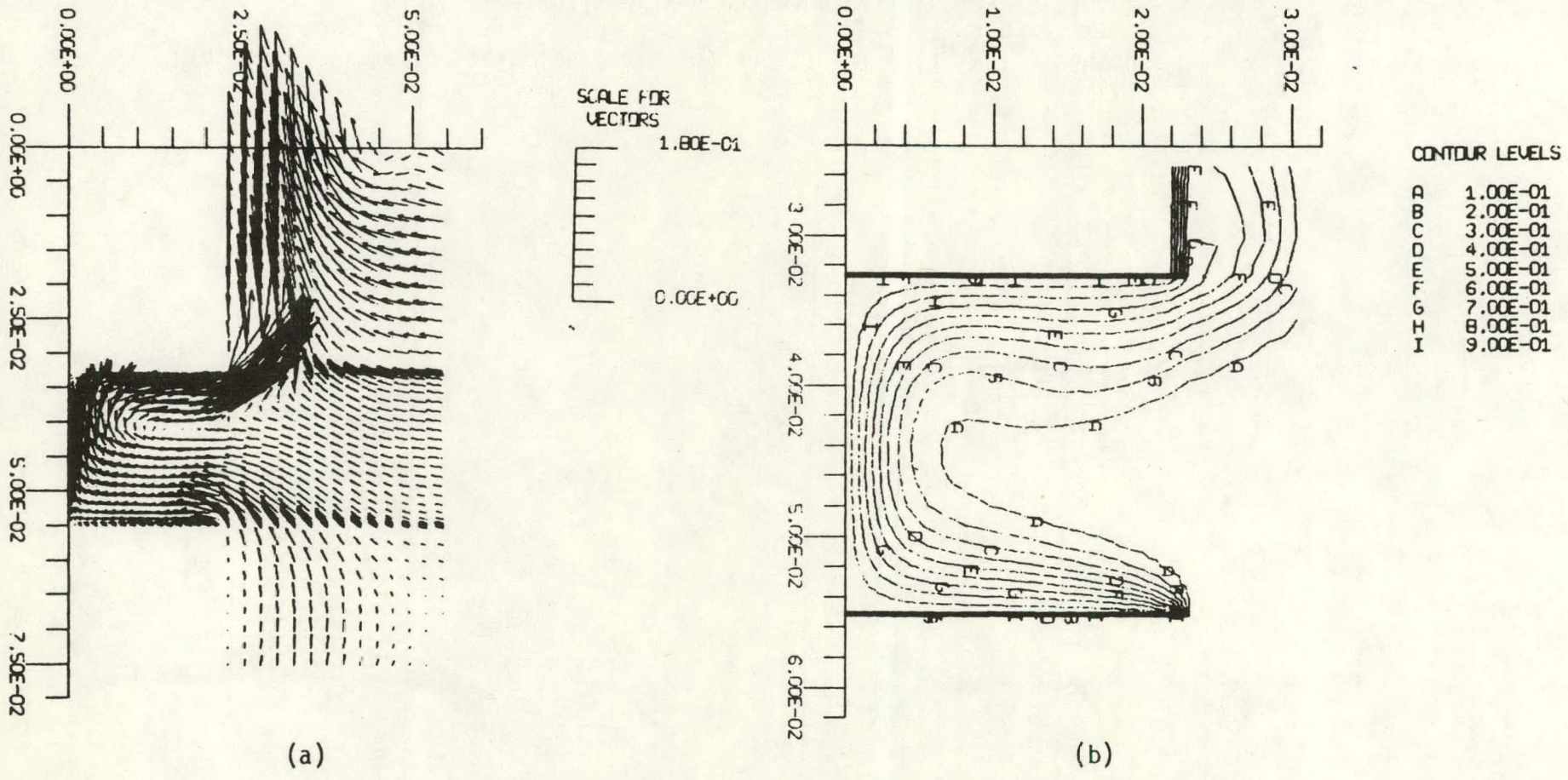

Fig. 3 Vector velocity field (a) and $(T - T_\infty)/(T_W - T_\infty)$ contours (b) for a/b = 1, $\alpha = 0°$, $Gr = 10^5$ and $T_W - T_\infty = 50°K$. Irrotational incompressible far-field boundary conditions specified for velocity gradients. Scale in m/s.

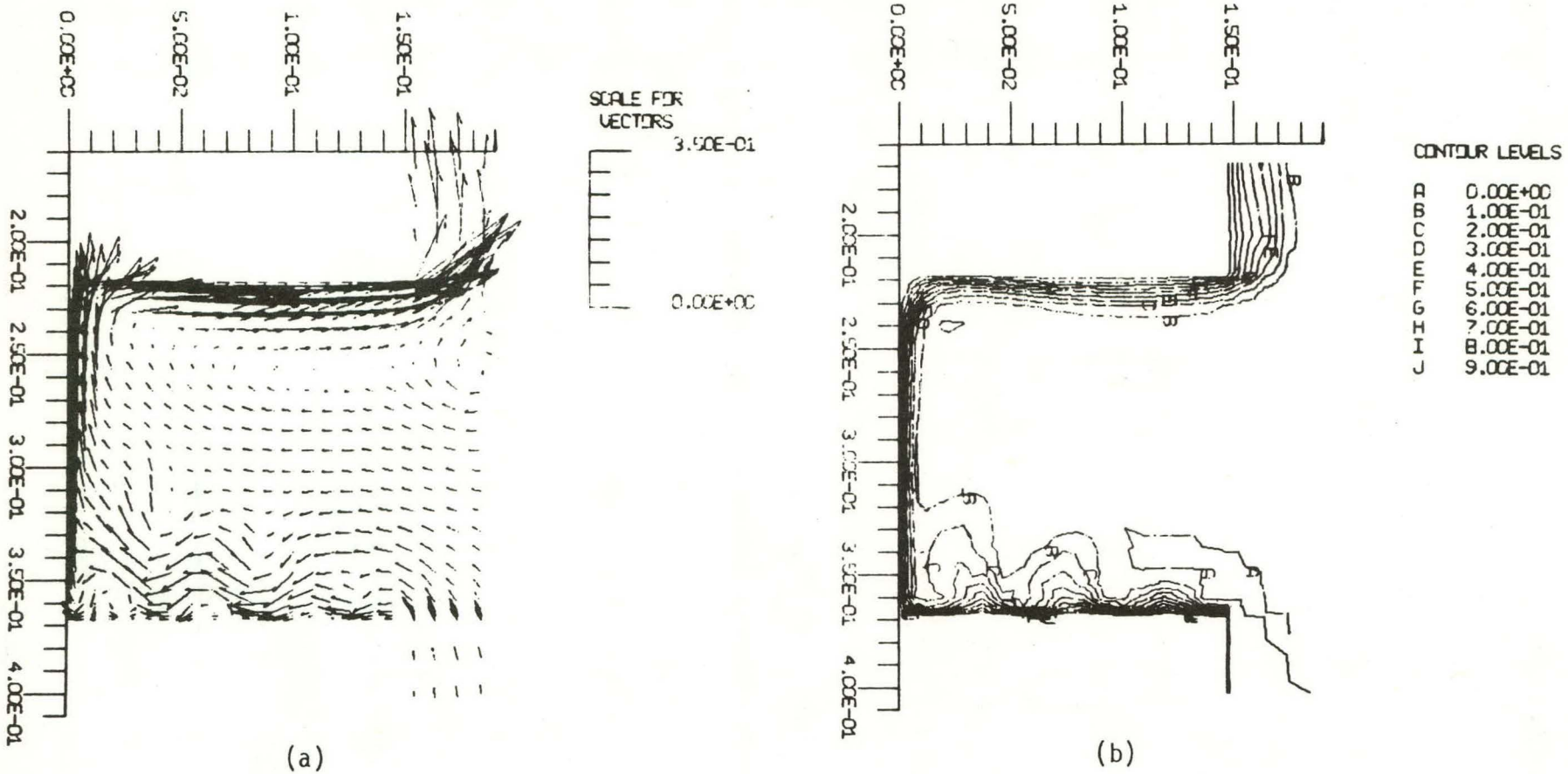

Fig. 4 Vector velocity field (a) and $(T - T_\infty)/(T_W - T_\infty)$ contours (b) for thermally-driven unsteady cavity flow at time $t = t_o$ in a cycle: $a/b = 1$, $\alpha = 0°$, $Gr = 3 \times 10^7$ and $T_W - T_\infty = 50°K$. Scale in m/s.

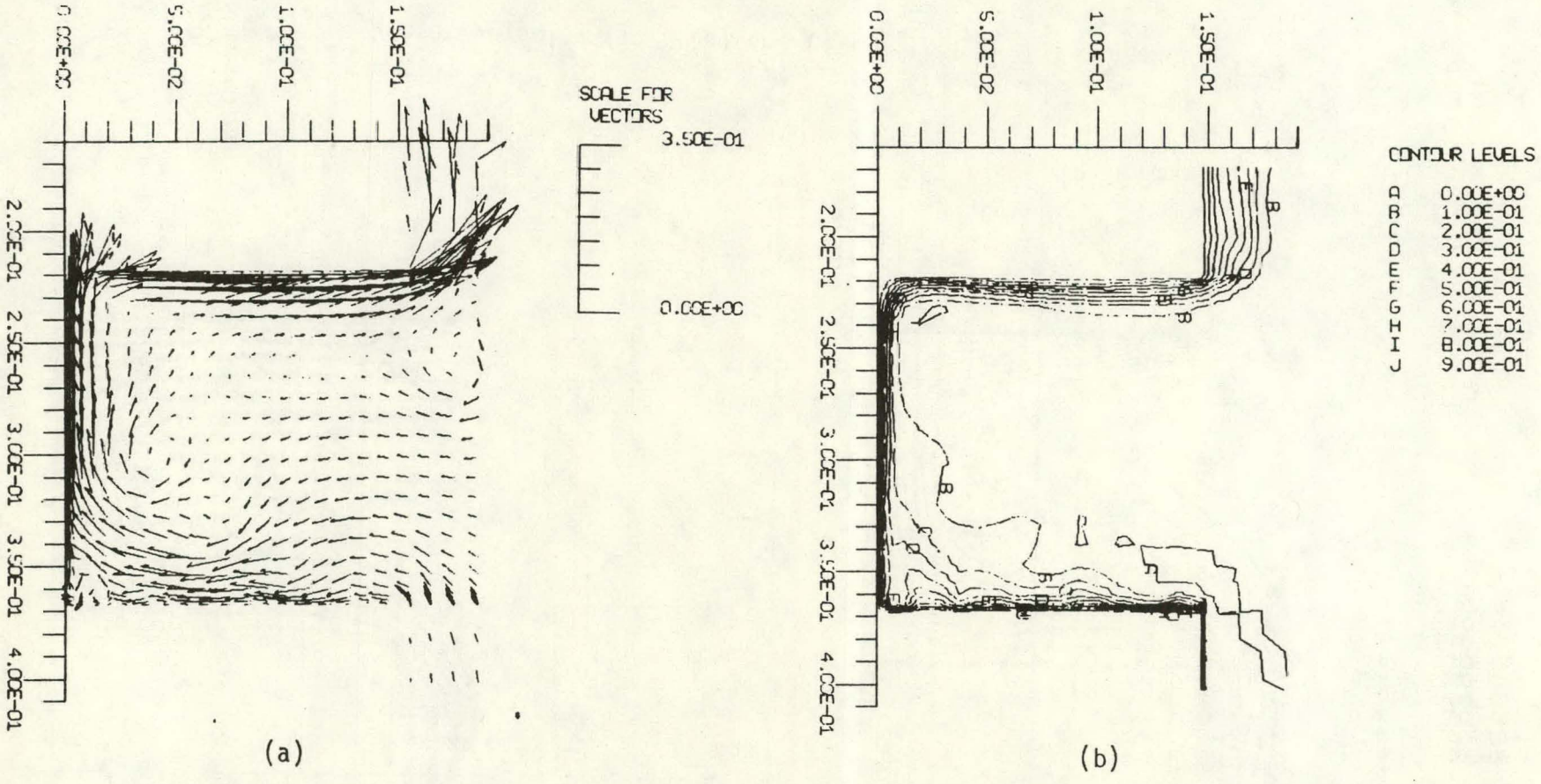

Fig. 5 Vector velocity field (a) and $(T - T_\infty)/(T_W - T_\infty)$ contours (b) for thermally-driven unsteady cavity flow at time $t = t_o + 2$ s in a cycle. Conditions given in Fig.4 . Scale in m/s.

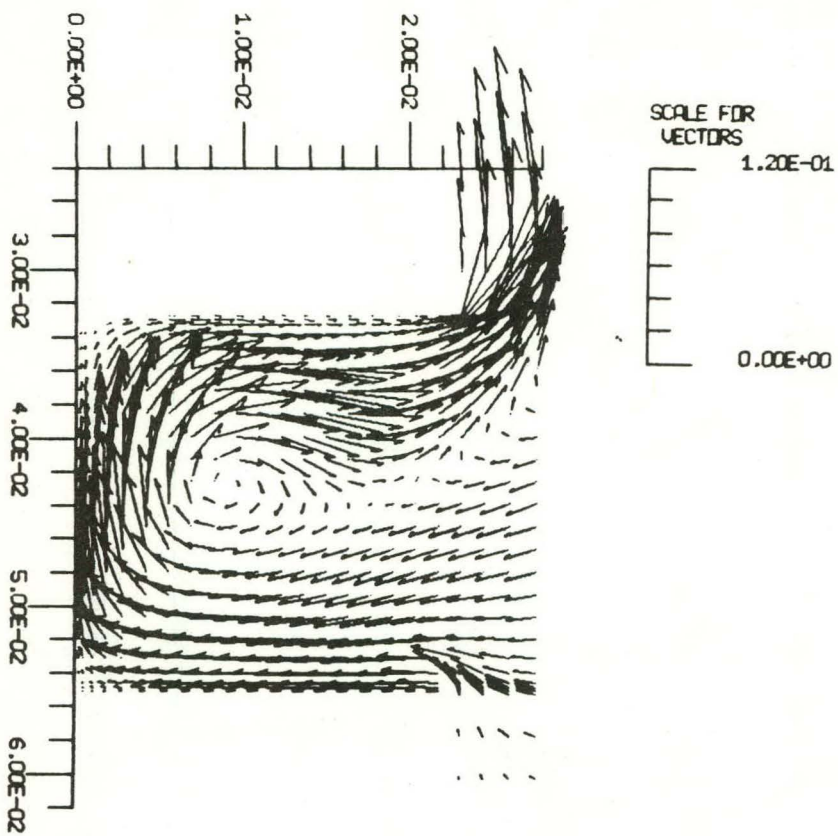

(a)

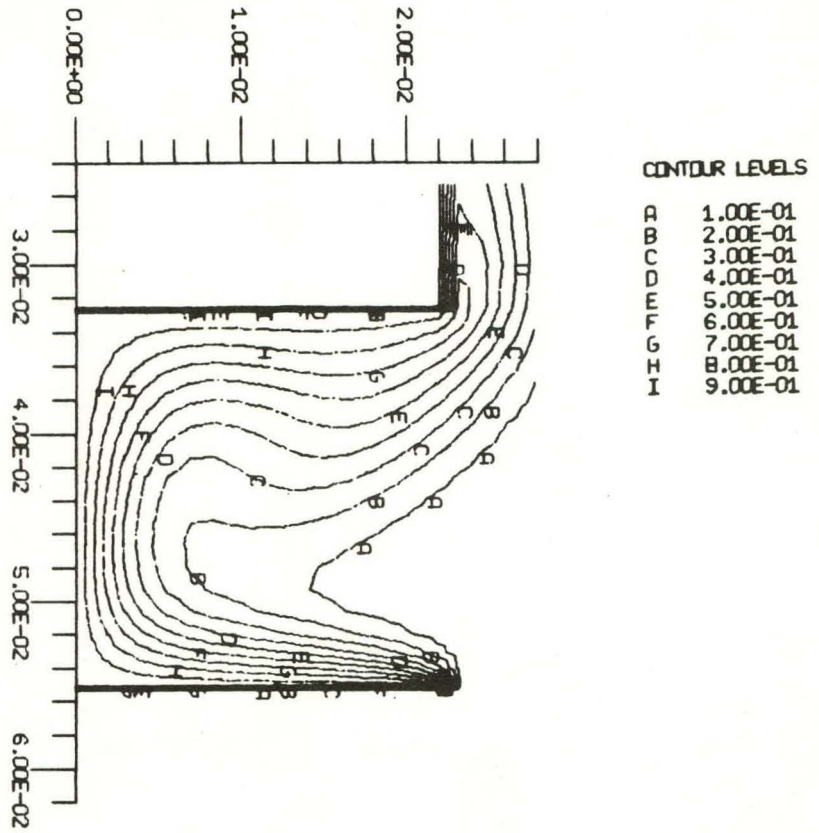

(b)

Fig. 6 Vector velocity field (a) and $(T - T_\infty)/(T_W - T_\infty)$ contours (b) for thermally-driven cavity flow: $a/b = 1$, $\alpha = 20°$, $Gr = 10^5$ and $T_W - T_\infty = 50°K$. Scale in m/s.

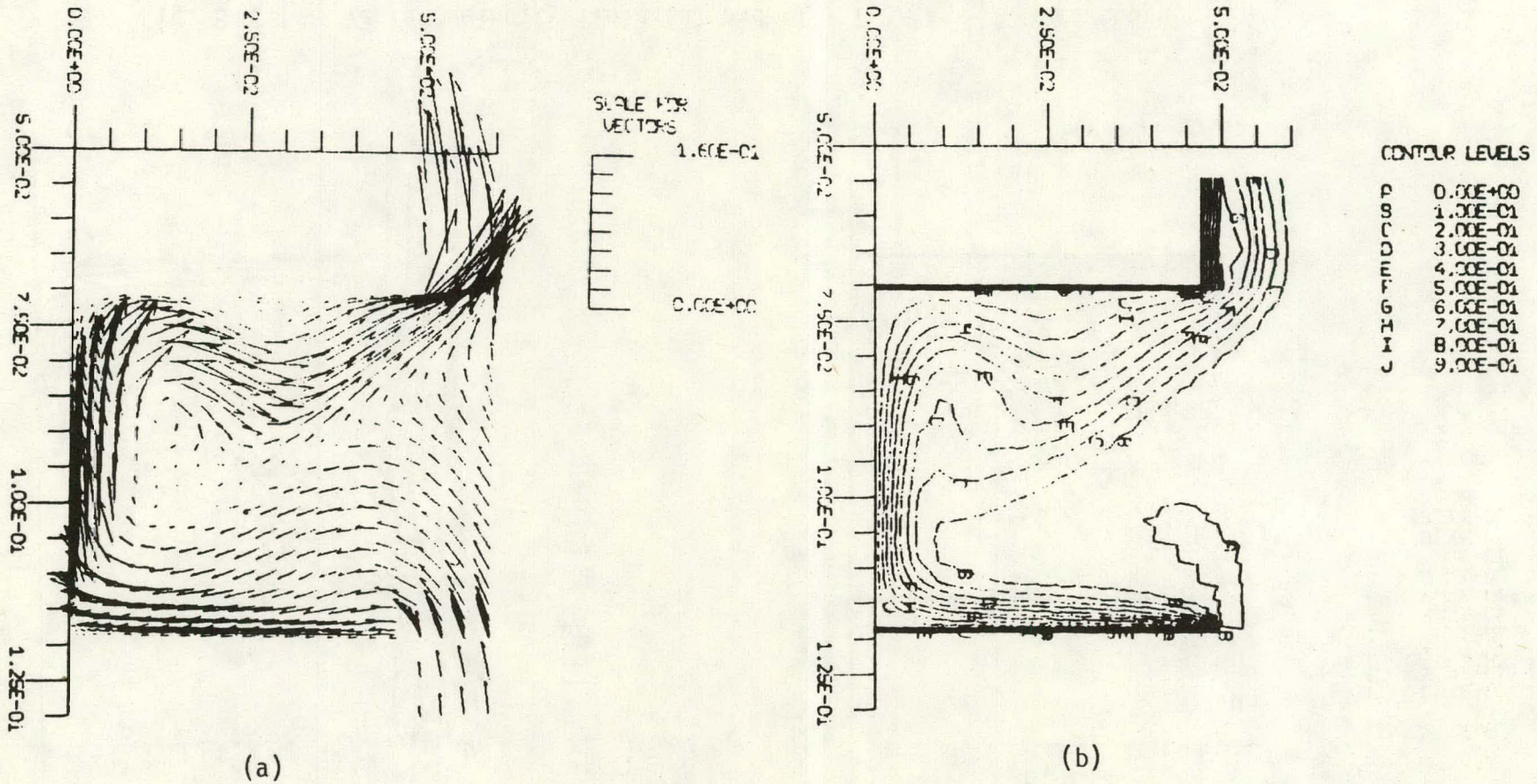

(a) (b)

Fig. 7 Vector velocity field (a) and $(T - T_\infty)/(T_w - T_\infty)$ contours (b) for thermally-driven cavity flow: $a/b = 1$, $\alpha = 20°$, $Gr = 10^6$ and $T_w - T_\infty = 50°K$. Scale in m/s.

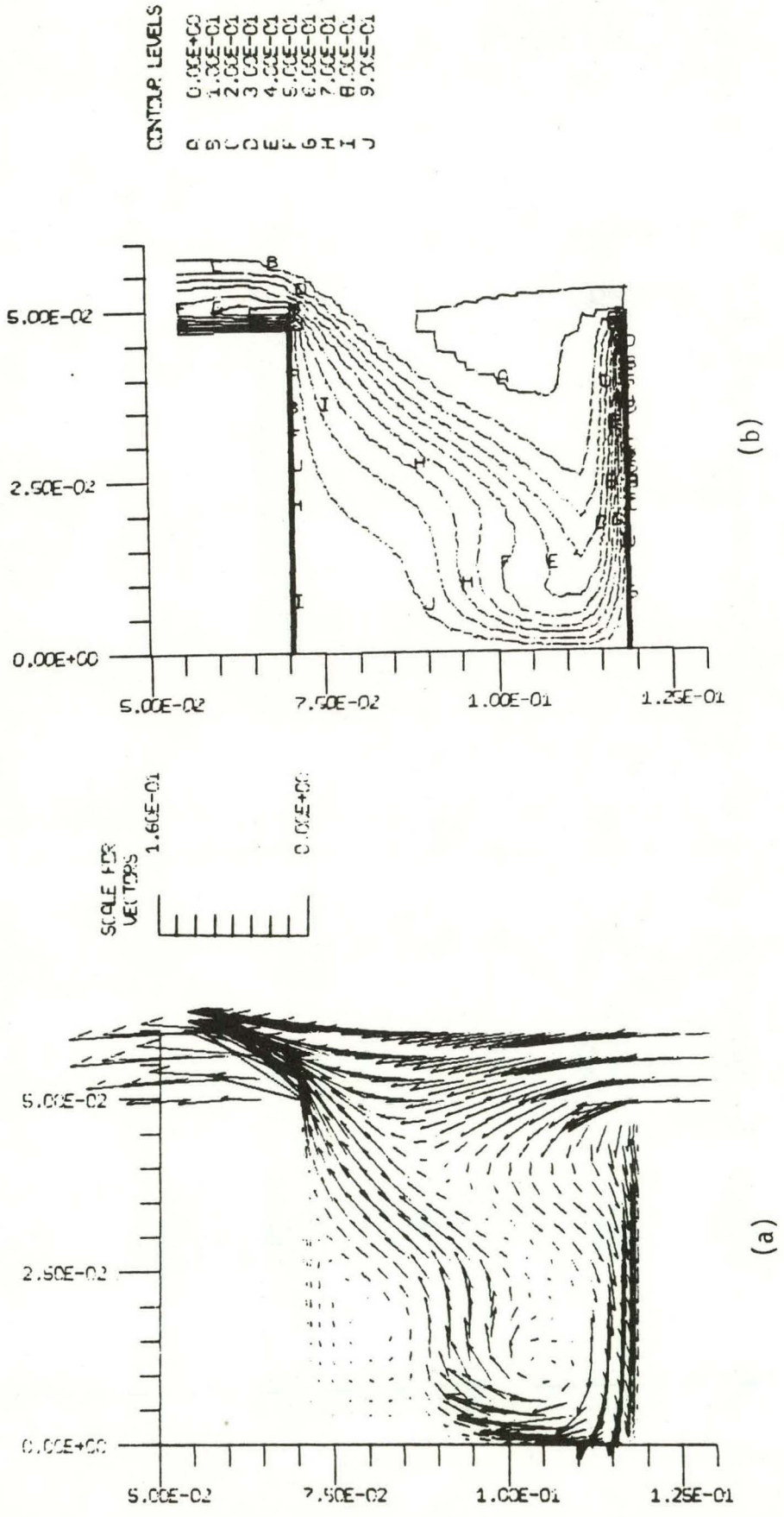

Fig. 8 Vector velocity field (a) and $(T - T_\infty)/(T_w - T_\infty)$ contours (b) for thermally-driven cavity flow: $a/b = 1$, $\alpha = 45°$, $Gr = 10^6$ and $T_w - T_\infty = 50°K$. Scale in m/s.

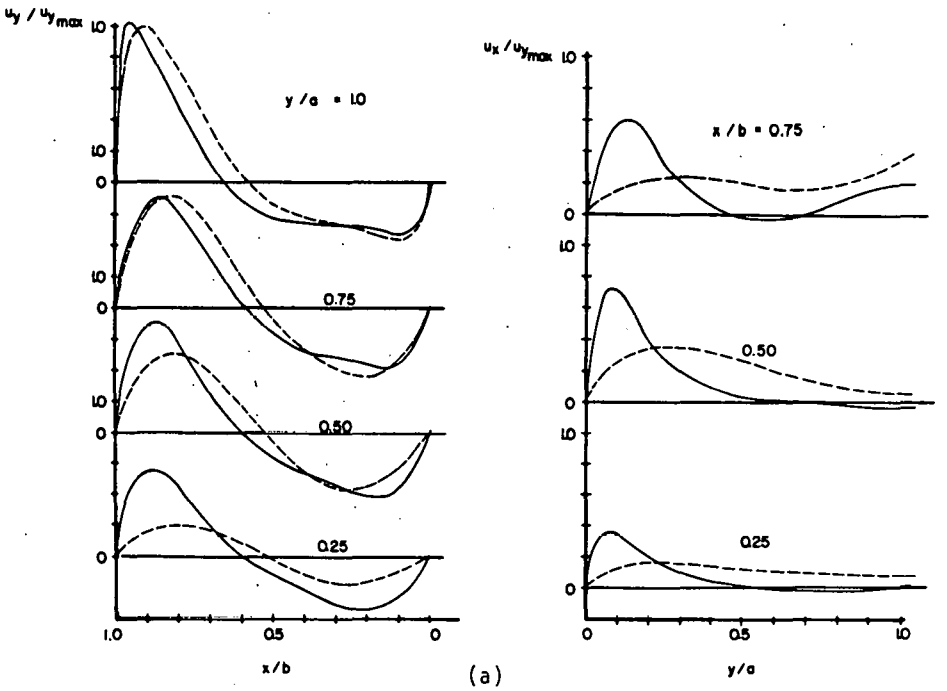

Fig. 9 Velocity (a) and temperature (b) profiles for thermally-driven cavity flow with a/b = 1, $\alpha = 0°$, $Gr = 10^5$ and;

i) $T_W - T_\infty = 50°K$, $u_{y_{max}} = 0.114$ m/s (———);

ii) $T_W - T_\infty = 500°K$, $u_{y_{max}} = 0.23$ m/s (- - -).

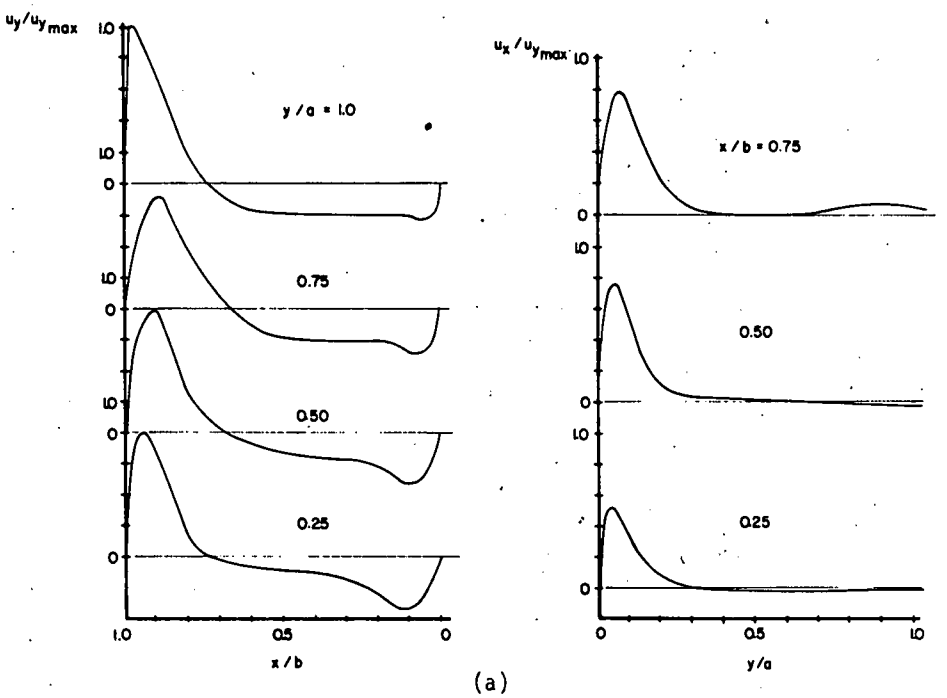

(a)

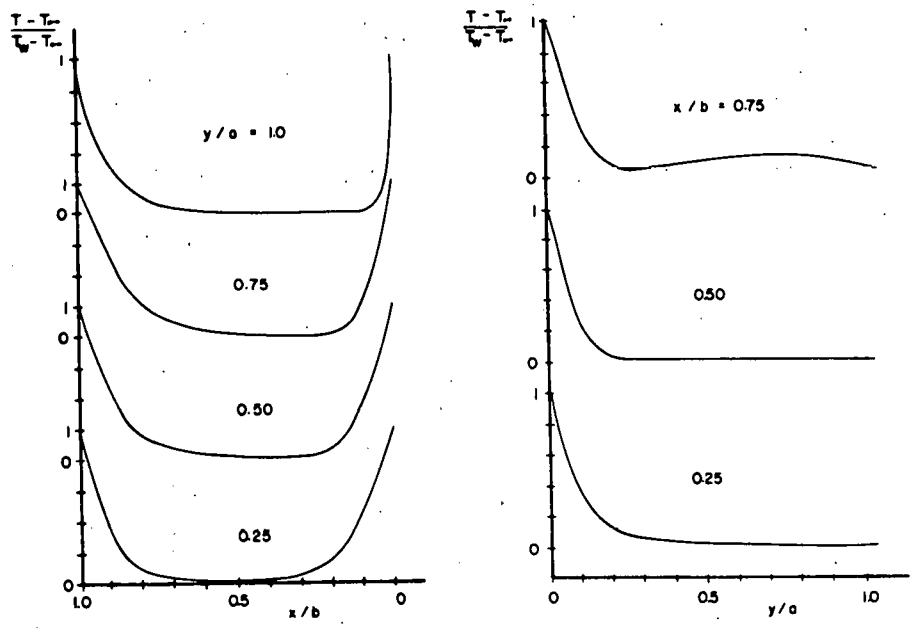

(b)

Fig. 10 Velocity (a) and temperature (b) profiles for thermally-driven cavity flow: a/b = 1, $\alpha = 0°$, $Gr = 10^6$ and $T_W - T_\infty = 50°K$; $u_{y_{max}} = 0.153$ m/s.

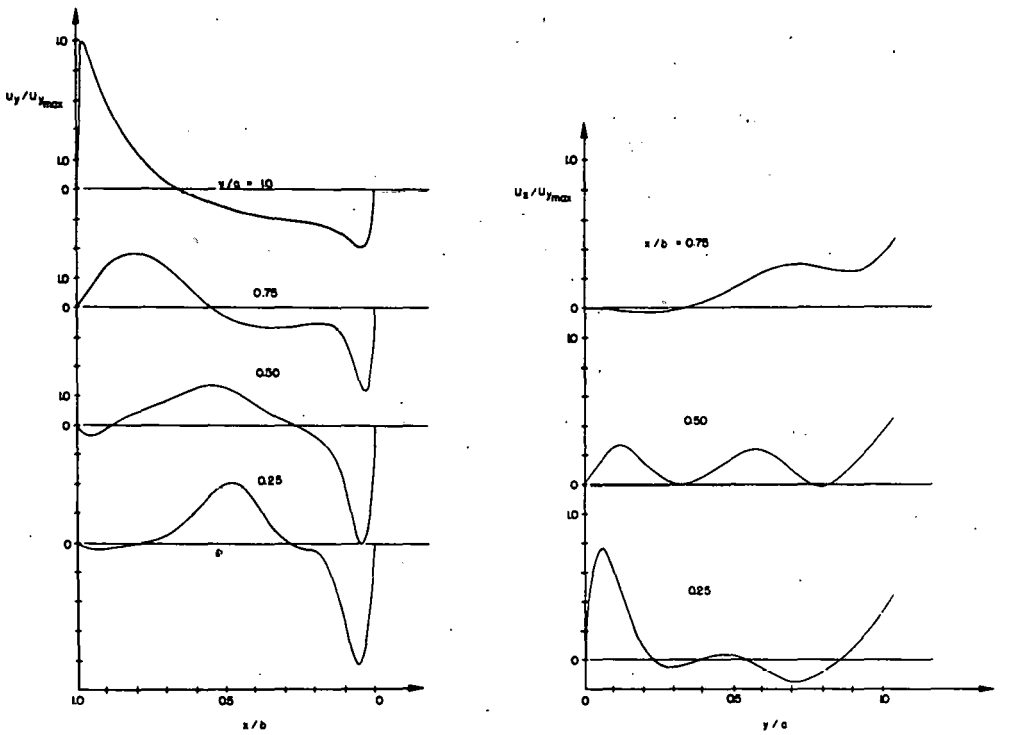

(a)

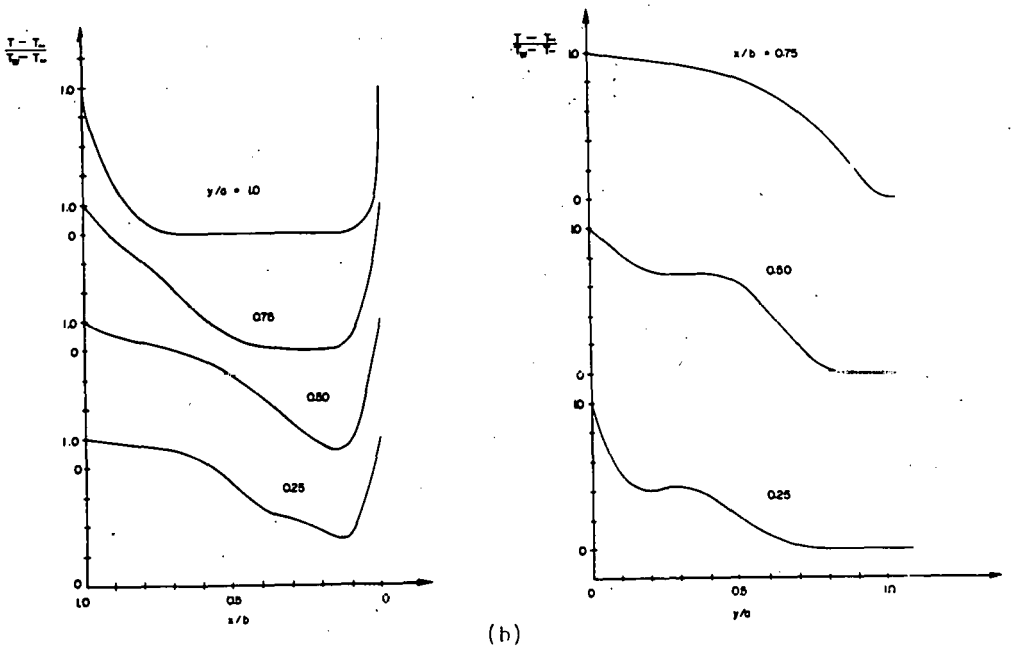

(b)

Fig. 11 Velocity (a) and temperature (b) profiles for thermally-driven cavity flow: a/b = 1, α = 45°, Gr = 10^6 and $T_w - T_\infty$ = 50°K; $u_{y_{max}}$ = 0.114 m/s.

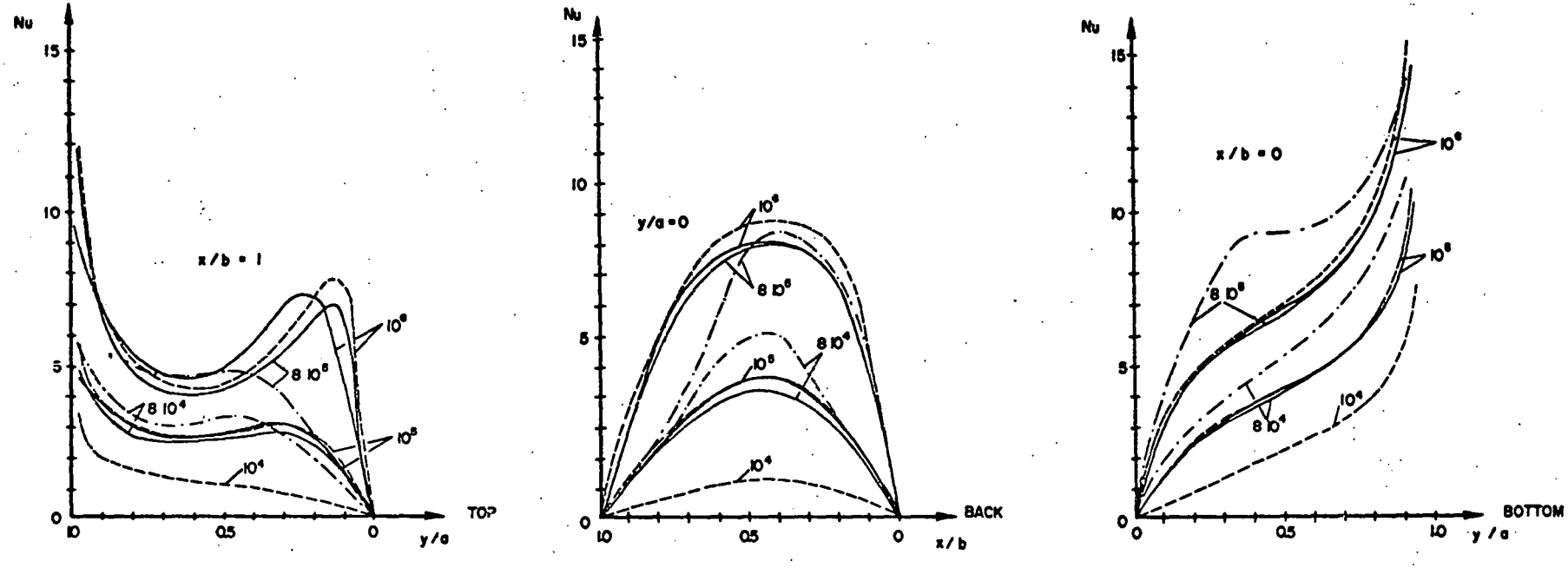

Fig. 12 Nusselt number at cavity walls: (———) QUICK, (- - - -) HYBRID, (— - —) data from Penot [3] .

INITIAL DISTRIBUTION

U.S. Department of Energy
Washington, D.C. 20545
Attn: J. E. Rannels
G. W. Braun
K. T. Cherian

Division of Solar Technology
U.S. Department of Energy
San Francisco Operations Office
1333 Broadway
Oakland, CA 94612
Attn: R. W. Hughey

Solar Energy Research Institute
1536 Cole Boulevard
Golden, CO 80401
Attn: B. P. Gupta
J. Lefferdo

Professor R. Greif
College of Engineering
Department of Mechanical Engineering
University of California, Berkeley
Berkeley, CA 94720

Professor R. Viskanta
School of Mechanical Engineering
Purdue University
West Lafayette, Indiana 47907

Professor O. Plumb
Department of Mechanical Engineering
Washington State University
Pullman, Washington

Professor J. A. C. Humphrey (3)
College of Engineering
Department of Mechanical Engineering
University of California, Berkeley
Berkeley, CA 94720

Professor E. Somerscales
Rensselaer Polytechnic Institute
College of Engineering
Troy, NY 12181

Dr. L. L. Eyler
Battelle Pacific Northwest Laboratories
P. O. Box 999
Richland, Washington 99352

Professor V. Sernas
Rutgers State University of New Jersey
College of Engineering
P. O. Box 909
Piscataway, NJ 08854

SRI International
333 Ravenswood Avenue
Menlo Park, CA 94025
Attn: A. J. Slemmons

Dr. P. Le Quere
Laboratoire D'Energetique Solaire
40 Avenue du Rector Pineau
86022 Poitiers
France

Professor F. S. Sherman
Department of Mechanical Engineering
University of California, Berkeley
Berkeley, CA 94720

D. B. Hayes, 5510; Attn: J. W. Nuziato, 5511
D. F. McVey, 5512
D. W. Larson, 5513
J. H. Scott, 4700; Attn: G. E. Brandvold, 4710
V. L. Dugan, 4720; Attn: W. P. Schimmel, Jr., 4723
T. B. Cook, 8000; Attn: A. N. Blackwell, 8200
B. G. Murphey, 8300
L. Gutierrez, 8400
D. L. Hartley, 8500
D. M. Olson, 8100; Attn: J. F. Barham, 8110
J. L. Wirth, 8150
R. D. Cozine, 8160

W. E. Alzheimer, 8120; Attn: G. A. Benedetti, 8121
C. S. Hoyle, 8122
W. D. Zinke, 8123

M. Abrams, 8124
R. J. Gallagher, 8124
R. C. Wayne, 8430
C. S. Selvage, 8450
A. F. Baker, 8452 (2)
A. C. Skinrood, 8452
E. T. Cull, Jr., 8453
W. G. Wilson, 8453 (5)
Publications Division, 8265, for TIC (27)
Publications Division, 8265/Technical Library Processes Division, 3141
Technical Library Processes Division, 3141 (3)
M. A. Pound, 8214, for Central Technical Files (3)